CDF/ANAL/EXOTIC/CDFR/9575
Version 1.1
November 3, 2008

Setting Limits on GMSB Models in the $\gamma\gamma + \not\!\!E_T$ Final State

Max Goncharov, Eunsin Lee, and Dave Toback
Texas A&M University
Ray Culbertson, Sasha Pronko
Fermilab

Abstract

We present the results of an optimized search for a gauge mediated supersymmetry breaking model with $\tilde{\chi}_1^0 \to \gamma\tilde{G}$ with $\tau(\tilde{\chi}_1^0) = 0$ ns in the $\gamma\gamma+\not\!\!E_T$ final state. We observed 1 event using 2.03 fb^{-1} of data collected by CDF II detector, which is consistent with the background estimate of 0.62 ± 0.29 events. We set cross section limits and mass limits as well as interpret our results for lifetimes up to 2 ns and find the exclusion region in the $\tilde{\chi}_1^0$ lifetime vs. mass plane with a mass reach of 138 GeV/c^2 at $\tau(\tilde{\chi}_1^0) = 0$ ns.

Contents

1 Introduction

The $\gamma\gamma$+$\not\!\!E_T$ final state is present in many theoretical models of new physics beyond the Standard Model (SM). An example of a theory that would produce these particles is gauge mediated supersymmetry breaking (GMSB) [1] with $\tilde{\chi}_1^0 \to \gamma\tilde{G}$ where the $\tilde{\chi}_1^0$ is the lightest neutralino and the next-to-lightest supersymmetric particle (NLSP) and $\tilde{G}$, a gravitino as the lightest supersymmetric particle (LSP). For much of parameter space GMSB model predicts $\tilde{\chi}_1^0 \to \gamma\tilde{G}$. The GMSB model is compelling for various reasons [2]. As the messenger interactions are flavor-independent it intrinsically suppresses flavor-changing, neutral currents and CP-violating processes to SM levels. It is also consistent with cosmological constraints [3] as all SUSY particles produced in the early universe decay to the $\tilde{G}$ LSP, which can be a warm dark matter candidate, depending on $\tilde{G}$'s mass [4]. Finally, this model naturally predicts high energy photon events at the Tevatron and gained favor with the appearance of the $ee\gamma\gamma\not\!\!E_T$ candidate event in run I [5].

For these models, current limits for collider experiments, astronomy and cosmology favor heavy $\tilde{\chi}_1^0$, with a mass above ∼100 GeV and a lifetime on the order of nanoseconds that decay to photons. At the Tevatron gaugino pair-production dominates and the decays produce $\tilde{\chi}_1^0$'s in association with jets, with each $\tilde{\chi}_1^0$ decaying into a $\tilde{G}$, that gives rise to $\not\!\!E_T$, and a photon. Depending on how many of the two $\tilde{\chi}_1^0$'s decay inside the detector, due to their large decay length, the event has the signature $\gamma\gamma$+$\not\!\!E_T$ or γ+$\not\!\!E_T$ with one or more additional jets.

In this note we focus on the optimization of the $\gamma\gamma$+$\not\!\!E_T$ search for GMSB models, which is more sensitive to lower $\tilde{\chi}_1^0$ lifetimes ($\tau < 5$ ns) [6]. The structure of this note is as follows: This section continues with a description of the GMSB models in more detail, summarizes the previous search [7] and provides an overview of our analysis and search strategy. Section 2 describes the dataset and the baseline event selection. Section 3 outlines the different backgrounds and how we estimate them for use in the optimization procedure. Section 4 describes the Monte Carlo (MC) that we use to model the signal acceptance and Section 5 gives the systematic uncertainties on the acceptance and the production cross sections. The optimization procedure, and its result, are given in Sec. 6. We unblind the signal region in Sec. 7, compare with expectations and set cross section, mass and lifetime limits. We conclude in Sec. 8 with expectations for the future.

1.1 Theory and Phenomenology

Supersymmetric models with GMSB [1] are characterized by a supersymmetry breaking scale Λ as low as 100 TeV and a light gravitino which is naturally the lightest supersymmetric particle. In GMSB models the standard model gauge interactions act as messengers of supersymmetry breaking if fields within the supersymmetry breaking sector transform under the standard model gauge group. In these models the NLSP is either the stau, $\tilde{\tau}$, or the $\tilde{\chi}_1^0$ depending on parameter choice [8]. We will focus on the $\tilde{\chi}_1^0$-NLSP case here, for which the branching ratio is ∼100% to decay to a photon and a $\tilde{G}$. Current limits restrict the masses of the squarks, gluons to be so large that they are too heavy to be produced at the Tevatron so gaugino pair-production channels dominate.

The minimal model of GMSB can be described in terms of the 6 free parameters listed in Table 1. For concreteness we use the Snowmass Slope constraint (SPS 8) [8] that is commonly used [7, 9] to reduce the number of free parameters from 6 to 2: the $\tilde{\chi}_1^0$ mass and lifetime. In some sense, one of the important parameters is Λ because it sets the overall mass scale of supersymmetric particles. To first approximation, all of the MSSM superpartner masses scale linearly with Λ. The gaugino-masses scale, N, is also very important because it determines which sparticle is the NLSP. For $N = 1$ the NLSP is mainly the lightest neutralino, and for $N \geq 2$ it is one of the sleptons. While

Λ	the effective SUSY breaking scale
M_m	the messenger mass scale
N	the number of messenger generations
$\tan\beta$	the ratio of the MSSM Higgs vacuum expectation values
sign(μ)	the sign of the Higgs sector mixing parameter
$C_{\tilde{G}}$	the ratio of the messenger sector

Table 1: The 6 parameters of the minimal model of GMSB.

the NLSP decay length scales like $C^2_{\tilde{G}}$ and also depends on $M_{\tilde{G}}$ [10], for much of the parameter space it is very small. For concreteness we use the Snowmass Slope constraint (SPS 8) [8] that is commonly used [7, 9] to reduce the number of free parameters from 6 to 2: the $\tilde{\chi}^0_1$ mass and lifetime[1]. The coupling to the gravitino is very weak, therefore, all the superparticles other than the NLSP undergo cascade decay down to the NLSP which finally decays to the gravitino.

At the Tevatron $\tilde{\chi}^0_1$'s are mostly pair produced as end products of cascade decays from a chargino, $\tilde{\chi}^\pm_1$, pair (∼45% of all channels) or a $\tilde{\chi}^\pm_1$ and a $\tilde{\chi}^0_2$ (∼25% of all channels) [11]. The major decay channels are shown in Fig. 1. For much of the parameter space the $\tilde{\chi}^0_1$ can be long-lived, with a decay time on the order of nanoseconds which corresponds to decay lengths of meters constrained by astronomy to have a $m_{\tilde{G}}$ near a keV [4]. The $\tilde{\chi}^0_1$ can decay inside the detector or, in a fraction of cases, leave the detector volume before it decays. This separates 3 event signatures: $\gamma\gamma$+$\not\!\!E_T$ γ+$\not\!\!E_T$ or $\not\!\!E_T$ each in association with jets from the τ's in the cascade decays. In this note we will focus on the $\gamma\gamma$+$\not\!\!E_T$ case as this is more sensitive to low lifetimes on the order of nanoseconds (2 ns), which is favored for large masses for cosmology regions [6].

Table 2 gives some example GMSB model parameters, the resulting $\tilde{\chi}^0_1$ mass and lifetime, and the next-to-leading-order (NLO) production cross section for our region of interest. The production cross sections are calculated to leading-order using PYTHIA [12] with the NLO corrections using the K-factors shown in Figure 2 as a function of $\tilde{\chi}^0_1$ masses for $\tilde{\chi}^\pm_1$ pair and $\tilde{\chi}^\pm_1\tilde{\chi}^0_2$ production taken from [13]. The values range around 1.1-1.3 for the mass range considered. The production cross section is independent of the $\tilde{\chi}^0_1$ lifetime, as this only scales with the $\tilde{G}$ mass for a fixed $\tilde{\chi}^0_1$ mass [1]. We use the total production cross section to estimate our sensitivity as it produces the best limits [14]. Next we outline our search strategy and the datasets.

1.2 Previous Searches

There have been many previous searches for anomalous $\gamma\gamma$+$\not\!\!E_T$ production including Run I searches from CDF [5] & DØ [15] and multiple searches from LEP II [9]. The most recent search from CDF in the $\gamma\gamma$+$\not\!\!E_T$ final state at CDF [7] with 202 pb^{-1} of data was performed in 2004. With zero observed events with $\not\!\!E_T$> 45 GeV in the data and the 18% systematic error we set a 3.3 event 95% C.L. upper limit on the expected number of signal events. Using the NLO predictions we set a limit of $M_{\tilde{\chi}^0_1} < 93$ GeV/c^2, assuming the $\tilde{\chi}^0_1$ lifetime is zero.

In 2006 the search [16] for a single photon with delayed arrival time, using the EMTiming

[1]The mass range $M_{\tilde{G}}$ between a few eV/c^2 and a few hundred eV/c^2 is favored for cosmological reasons and typically produces a neutralino lifetime of less than a few hundred nsec depending on the NLSP mass. This parameter is important because the lifetime determines whether the NLSP decays inside or outside the detector. For more discussion of the issues and details of prospects of searches with long-lived neutralinos-NLSPs which decay to $\gamma\tilde{G}$ see Ref. [6].

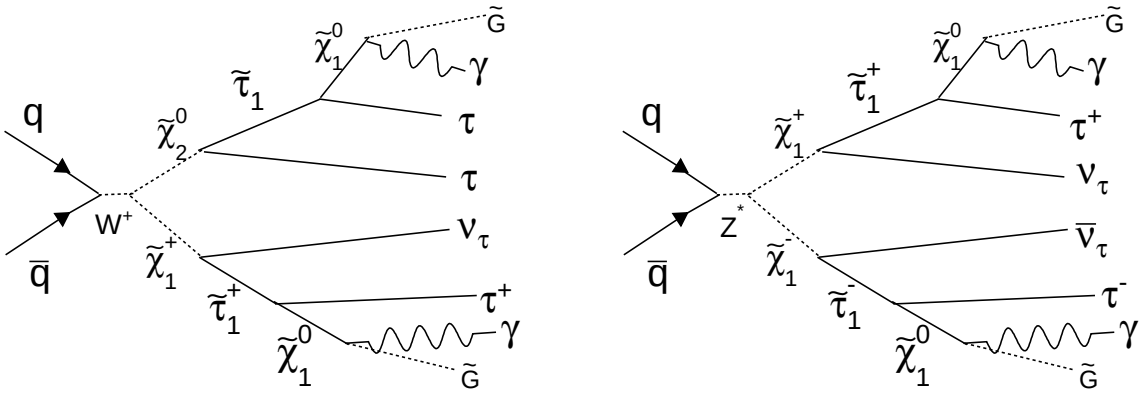

Figure 1: Feynman diagrams of the dominant tree production processes at the Tevatron for the GMSB model line we consider: $\tilde{\chi}_1^{\pm}\tilde{\chi}_2^0$ (45%) (a) and $\tilde{\chi}_1^{\pm}$ pair (b) production (25%). The τ's and second photons, if available, can be identified in the calorimeter as jets. Note that we only show one choice for the charge. The remaining processes are slepton (τ_1, e_R, μ_R) pair production.

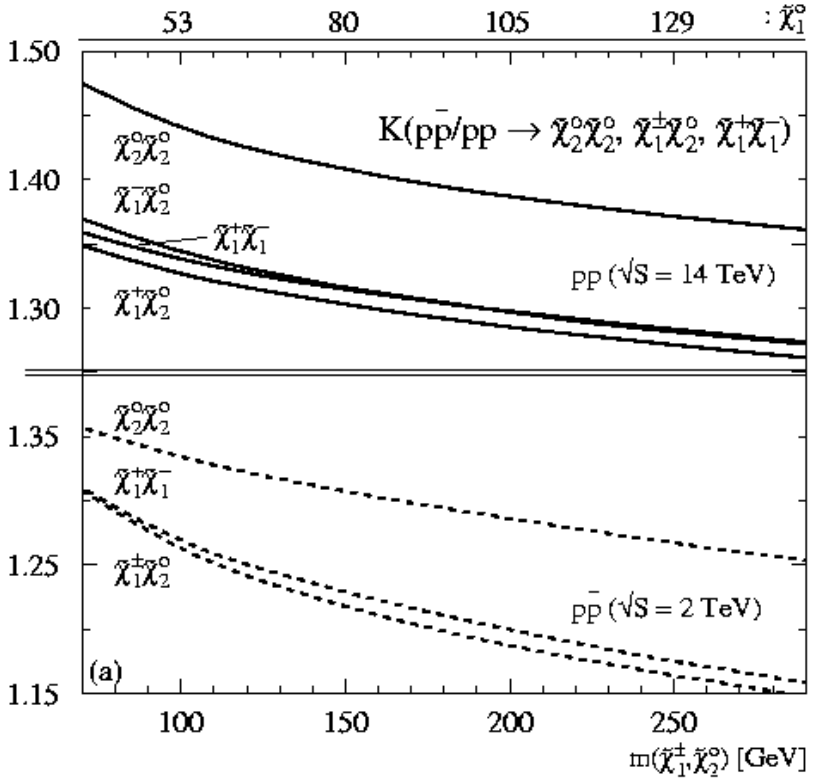

Figure 2: The K-factors for use in modifying the LO production cross sections of $\tilde{\chi}_1^{\pm}$ pair and $\tilde{\chi}_1^{\pm}\tilde{\chi}_1^0$ production from PYTHIA as a function of the average mass of the $\tilde{\chi}_1^{\pm}$ and $\tilde{\chi}_2^0$ which are almost identical in the scenario chosen in Ref. [8]. The figure is taken from Fig. 3a. For convenience the $\tilde{\chi}_1^0$ mass is plotted as a second x-axis, also taken from Fig. 3b of Ref. [13].

$m_{\tilde{\chi}_1^0}$ (GeV/c^2)	$\tau_{\tilde{\chi}_1^0}$ (ns)	$m_{\tilde{G}}$ (eV/c^2)	Λ (GeV)	K-factor	NLO σ_{prod} (fb)
70	0	1.38	53550	1.23	999.9
90	0	2.18	67250	1.20	286.8
100	0	2.63	74000	1.19	169.0
130	0	4.34	95000	1.16	36.23
130	2	317	95000	1.16	36.23
140	0	4.99	101850	1.15	22.97

Table 2: Examples for $\tilde{\chi}_1^0$ masses and lifetimes relevant for this analysis and their translation to the SUSY parameters in accordance with the GMSB Snowmass Slope SPS 8 [8], and the NLO production cross sections. The production cross section only scales with the $\tilde{G}$ mass for a fixed $\tilde{\chi}_1^0$ mass [1]. Note the different unit for the $\tilde{G}$ mass.

system [17], at least one jet, and $\not\!\!E_T$, at CDF sets the most stringent limits on GMSB in the signature, which is more sensitive to higher lifetimes. The search found 2 events using 570 pb^{-1} of data that is consistent with the background estimate of 1.3±0.7 events. Figure 3 shows the exclusion region in the $\tilde{\chi}_1^0$ lifetime vs. mass plane with a mass reach of 101 GeV/c^2 at $\tau_{\tilde{\chi}_1^0} \sim$5 ns. This results extended the world sensitivity to these models beyond those from LEP II [9], which allowed non-zero $\tilde{\chi}_1^0$ lifetime using photon pointing.

The current most sensitive search for GMSB with $\tau = 0$ is from DØ using 1.1 fb^{-1} of data [18]. The observed upper limits are $M_{\tilde{\chi}_1^0} < 125$ GeV/c^2.

1.3 Overview of the Analysis

This analysis is designed to optimize the limits on GMSB model in the $\gamma\gamma + \not\!\!E_T$ final state with $\tau = 0$. Our search is designed to identify the cascade decays from $\tilde{\chi}_1^\pm$ and/or $\tilde{\chi}_2^0$. The new features of our analysis since the last $\gamma\gamma + \not\!\!E_T$ search with 202 pb^{-1} are the following:

- Use EMTiming system to reject cosmic rays, beam halo, and PMT spikes.
- Use a new *Met Resolution Model* [19] to improve QCD background rejection.
- Simplify analysis due to more direct ways of rejecting backgrounds.
- Use 10 times the data (2 fb^{-1}).
- Extend the search to non-zero lifetimes.

We examine events with two isolated, central ($|\eta| \lesssim 1.0$) photons with $E_T > 13$ GeV for the presence of significant $\not\!\!E_T$. All candidates are required to pass global event selection, photon ID, and non-collision background rejection requirements. These requirements define our pre-selection sample. The final signal region is defined by further kinematic cuts and selected to optimize the rejection of the remaining backgrounds, QCD events ($\gamma\gamma$, $\gamma - jet \rightarrow \gamma\gamma_{fake}$ and $jet - jet \rightarrow \gamma_{fake}\gamma_{fake}$) with fake $\not\!\!E_T$ due to energy mis-measurement, events with real $\not\!\!E_T$ (e.g., $W\gamma \rightarrow \nu + e, \tau + \gamma \rightarrow \nu\gamma_{fake}\gamma$), and non-collision backgrounds such as PMT spikes, cosmic rays, and beam-halo (B.H.) interactions.

We perform a blind analysis in the sense that we blind the signal region and select the final event requirements based on the signal and background expectations alone. In Section 6 we optimize

our predicted sensitivity using a simulation of our GMSB model (see Section 4) and calculate, for each GMSB parameter point the lowest, expected 95% C.L. cross section limit as a function of the following event variables: $\not\!\!E_T$ *Significance*, H_T, and $\Delta\phi(\gamma_1, \gamma_2)$. After the optimization we are left with an optimal, robust set of requirements that define the signal region.

In addition to setting limits on $\tau = 0$ decays, we investigate our sensitivity for the lifetime region $\tau \sim 1$ ns to complement the delayed photon analysis [16]. As shown in Figure 3 there is an uncovered region below about a ns.

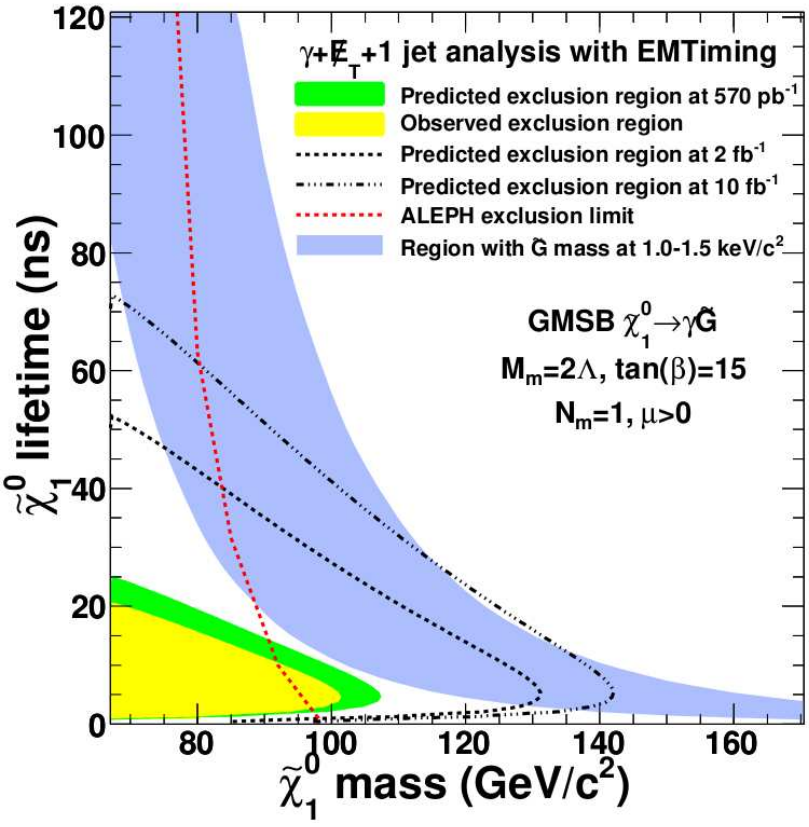

Figure 3: The predicted and observed exclusion region from the delayed photon search [16], along with cosmology favored region and the exclusion limit from ALEPH/LEP [9].

2 Triggers, Datasets and Object ID

In this section we describe the trigger, dataset, and the object ID used for the baseline selection. The analysis is based on data collected from the beginning of Run II and up to March 31, 2007. The integrated luminosity is obtained from the offline database and is scaled by a 1.019 correction factor [20]. To ensure the quality of data, the good run list v.17 [21] for the *Photon* group is applied. It requires good CAL, SMX, COT (COT degraded period is allowed, but Silicon is required during that period). After all requirements we are left with 2.034±1.22 fb^{-1} of data [22].

To get the pre-selection sample we apply diphoton triggers, photon ID, phoenix rejection, vertex requirement, and non-collision removal cuts. Next we describe these in detail.

2.1 Triggers and Datasets

The events used in this analysis are required to pass the DIPHOTON_12 (iso) or DIPHOTON_18 (non-iso) triggers [23]. The trigger requirements are listed in Table 3. The $\gamma\gamma + X$ data are "ntuplized" in the "cdfpstn:cdipad,h,i,j" Stntuples. We use the Stntuple dev_243 [24] and version 6.1.4 of the cdfsoft2 release.

DIPHOTON_12	
L1	Single tower $E_T > 8$ GeV $(z = 0)$ Single tower Had/EM< 1.25 or $E_T > 14$
L2	Two high E_T pass clusters, $E_T > 10$ $(z = 0)$, $\eta < 3.6$ Both clusters Had/EM < 1.25 Both clusters Iso < 3 || Iso $< 0.15E_T$
L3	Two L3 clusters, $E_T > 12$ $(z = 0)$ Both clusters Had/EM $< 0.055 + 0.00045E$ || $E_T > 200$ Both clusters Iso(cone 0.4) < 2 || $< 0.10E_T$ for central, average and scaled CES $\chi^2 < 20$
DIPHOTON_18	
L1	Single tower $E_T > 8$ GeV $(z = 0)$ Single tower Had/EM< 1.25 or $E_T > 14$
L2	Two high E_T pass clusters, $E_T > 16$ $(z = 0)$, $\eta < 3.6$ Both clusters Had/EM< 1.25
L3	Two L3 clusters, $E_T > 18$ $(z = 0)$ Both clusters Had/EM $< 0.055 + 0.00045E$ || $E_T > 200$ for central, average and scaled CES $\chi^2 < 20$

Table 3: The diphoton triggers used to create the diphoton sample.

2.2 Diphoton Samples and Object ID

Diphoton candidate events are selected from the sub-sample of events that pass the trigger, and require both leading photons to be in the central, $|\eta| \leq 1.1$, pass the standard photon ID requirements and have $E_T^\gamma > 13$ GeV. The full set of requirements are given in Table 4.

In addition to the standard photon ID cuts we have added additional cuts to suppress PMT spikes [25]. PMT spikes in the CEM calorimeter can produce a fake photon signature and give fake

The Standard Tight Photon ID Cuts	
detector	CEM
corrected E_T	$\geq$ 13 GeV
CES fiduciality	$\lvert X_{\rm CES}\rvert \leq 21$ cm 9 cm $\leq \lvert Z_{CES}\rvert \leq 230$ cm
average CES χ^2	$\leq$20
Had/Em	$\leq 0.055+0.00045\times E$
corrected CalIso0.4	$\leq 0.1\times E_T$ if $E_T<$20 GeV or $\leq 2.0+0.02\times(E_T-20)$
TrkIso0.4	$\leq 2.0+0.005\times E_T$
$N3D$ tracks in cluster	≤ 1
track P_T if $N3D=0$	$\leq 1.0+0.005\times E_T$
E_T of 2^{nd} CES cluster (wire and strip)	$\leq 0.14\times E_T$ if $E_T<$18 GeV $\leq 2.4+0.01\times E_T$ if $E_T\geq$18 GeV
Additional Photon ID Cuts	
PMT Asymmetry	$A=\lvert pmt1-pmt2\rvert/(pmt1+pmt2)<0.65$
Phoenix	Matched to Phoenix Track

Table 4: Summary of the standard photon ID (tight) cuts in addition to the extra PMT asymmetry and Phoenix rejection cuts.

$\not\!\!E_T$. To suppress this background, we remove events with a large PMT asymmetry: $A=|pmt1-pmt2|/(pmt1+pmt2)$, where $pmt1$ and $pmt2$ are signals from PMT-1 and PMT-2, respectively.

Since a second source of background with large real $\not\!\!E_T$ is $e\gamma+X\rightarrow\gamma\gamma_{fake}+X$ events where an electron fakes a prompt photon we have added phoenix rejection cuts [26]. In many cases such a photon is either due to a bremsstrahlung in the detector material in front of the COT or due to a lost track (see Ref. [26] for details). These electrons usually leave a few silicon hits and can be reconstructed by Phoenix tracking algorithm. To reduce contamination by $e\gamma$ events, we reject events where a photon is matched to a phoenix track.

To help maintain the projective nature of the calorimeter we select events with at least one vertex of class 12 with $|z_{vx}|\leq$60 cm. The E_T of all calorimeter objects (individual towers, photons, electrons, and jets) are calculated with respect to the highest $\sum P_T$ (best) vertex.

Additional topology cuts are placed to reduce non-collision backgrounds. Muons from beam halo are known to fake the photon signature [25]. Because such events are not related to a hard interaction and usually appear only in one calorimeter wedge, they also create a large $\not\!\!E_T$. To suppress contribution due to this background, we use the standard beam halo ID cuts in Table 5 and the rejection procedure in [25, 27].

Cuts	values
seedWedge	>9
NHadPlug	>2
seedWedgeHadE	$<[0.4+(0.019(N_{vx12}-1)+0.013)seedWedge]$ GeV
wedge number	0 or 23

Table 5: Summary of beam halo ID cuts.

Run Range	Cosmic Ray Cuts
Before 190851	muon co-stub cut ($\Delta\phi(\mu - stub, \gamma) > 30\,^\circ$)
After 190851	EMTiming cut ($\|T\| > 4\sigma_T$, where $\sigma_T = 1.665$ ns and $\|\Delta T_{1,2} = T_1 - T_2\| > 4\sigma_{\Delta T}$, where $\sigma_{\Delta T} = 1.021$ ns)

Table 6: Summary of the cosmic ray cuts for different run ranges

A cosmic ray muon that traverses the detector often also creates a muon stub with a nearby energy deposit in the calorimeter. To suppress contributions from cosmic ray sources, we use different approaches for data before and after the EMTiming system [17] became available (run 190851). For data collected before run 190851, we reject events where there is a trackless muon stub in a cone of 30 ° around the direction of any of the two leading photons. For data with EMTiming system, we apply the timing cuts to reduce the contamination due to cosmic rays [25, 27]. The cosmic ray rejection cuts are listed in Table 6.

After all cuts our pre-selection sample consists of 32,720 events left after all the quality, ID and cleanup cuts are applied. Table 7 gives a summary of the event reduction.

Requirements	Signal sample (events passed)
Trigger, Goodrun, and Standard photon ID with $\|\eta\| < 1.1$ and $E_T > 13$ GeV	36,802
Phoenix rejection	33,899
PMT spike rejection	33,796
Vertex cuts	32,899
Beam Halo rejection	32,890
Cosmic rejection (EMTiming cut, after run 190851)	32,865
Cosmic rejection (Muon stub cut, before run 190851)	32,720
Total events passed	32,720

Table 7: Summary of $\gamma\gamma + \not\!\!E_T$ pre-sample selection requirements. Note we appy two different types of cosmic rejection cuts. EMTiming cuts are used to remove cosmic rays for data collected after run 190851 when EMTiming system installed and events where there is a trackless muon stub in a cone of 30 ° around the direction of any of the two leading photons before then.

3 Backgrounds

3.1 Overview

The final signal region for this analysis is defined by the subsample of pre-selection events that also passes a set of optimized final kinematic cuts. The methods for determining the background in the signal region are based on a combination of data and MC and allow for a large variety of final sets of cuts. We use these estimates as part of the optimization procedure described in Section 6. In this section we describe the backgrounds and the methods used to estimate the background rates and their uncertainties.

There are five major sources of background for $\not\!\!E_T$ in $\gamma\gamma$ events:

- QCD events with fake $\not\!\!E_T$:
  True $\gamma\gamma$, $\gamma - jet \rightarrow \gamma\gamma_{fake}$, and $jet - jet \rightarrow \gamma_{fake}\gamma_{fake}$ events where $\not\!\!E_T$ arises due to energy mis-measurement in the calorimeter.

- Electroweak events with $e\gamma$ and intrinsic $\not\!\!E_T$:
  Many Standard Model processes with electrons in the final state have intrinsic $\not\!\!E_T$ such as inclusive $W \rightarrow e\bar{\nu}$ production, $b \rightarrow e\bar{\nu}X$, or $\tau \rightarrow e\bar{\nu}_e\nu_\tau X$. In this case, typically, the electron track is lost. The second photon can be real or fake.

- Non-collision events:
  PMT spikes, cosmic ray or beam-halo events where one or more of the photons and $\not\!\!E_T$ are not related to the collision.

- Wrong vertex:
  Events where one or both photon candidates are coming from the vertex other than the highest $\sum P_T$ primary vertex, causing a large mis-measurement of the $\not\!\!E_T$.

- Tri-Photon:
  Events with a lost photon that creates the fake $\not\!\!E_T$.

We next discuss each in detail, how it is estimated and how the uncertainties are calculated.

3.2 QCD Backgrounds

Standard Model QCD events, $\gamma\gamma$, $\gamma - jet \rightarrow \gamma\gamma_{fake}$, and $jet - jet \rightarrow \gamma_{fake}\gamma_{fake}$, are the dominent sources of events in the diphoton final state and a major background for $\gamma\gamma + \not\!\!E_T$. The energy fluctuations, which lead to considerable values of fake $\not\!\!E_T$, happen only in small fraction of cases, but huge cross sections of these processes make them one of the largest backgrounds. However, we can significantly reduce the QCD background by selecting events based on $\not\!\!E_T$ $Significance$ using a new *Met Resolution Model* [19].

The *Met Resolution Model* considers the clustered and unclustered energy in the event and calculates a probability, $P(\not\!\!E_T{}^{fluct} > \not\!\!E_T)$, for fluctuations in the energy measurement to produce $\not\!\!E_T{}^{fluct}$ equivalent to or larger than the measured $\not\!\!E_T$. This probability is then used to define a $\not\!\!E_T$ $Significance$ as $-\log_{10}\left(P_{\not\!\!E_T{}^{fluct} > \not\!\!E_T}\right)$. Events with true and fake $\not\!\!E_T$ of the same value should have, on average, different $\not\!\!E_T$ $Significance$. By construction a $\not\!\!E_T$ $Significance$ cut of 3, 4, and 5 allows $\sim$0.1%, $\sim$0.01%, and $\sim$0.001% of QCD events.

This model assumed only two sources of mis-measurements that cause fake $\not\!\!E_T$: soft, unclustered energy (underlying event or multiple interactions), and jet energy clusters (jets). Measurements of both are defined in [19]. The unclustered energy tends to be uniformly spread in the calorimeter. Therefore, the portion of $\not\!\!E_T$ due to this source is usually small. Jets, unlike the soft energy, are collimated sprays of energetic particles in a certain direction. Because of the nature of jets, they tend to produce most of $\not\!\!E_T$.

We also use a sample of $Z/\gamma^* \rightarrow e^+e^-$ events to evaluate QCD background with fake $\not\!\!E_T$. To estimate the expected $\not\!\!E_T$ *Significance* for a sample (the number of events above a given $\not\!\!E_T$ *Significance* cut, we consider the jets and unclustered energy in the event and for each data event, we throw 10 pseudo-experiments to generate $\not\!\!E_T$ and calculate its significance according to the jets and underlying event configuration. Then we count the number of pseudo-experiments that pass our $\not\!\!E_T$ *Significance* cuts. This number devided by the number of pseudo-experiments gives us a prediction for the QCD background for a sample due to energy mis-measurements. In this way for any set of kinematic cuts for any sample we can predict the $\not\!\!E_T$ *Significance* distribution. After estimating this background, the expected $\not\!\!E_T$ *Significance* distributions of QCD is shown in Figure 8.

The systematic uncertainty on the number of QCD events in the final signal region is due to uncertianties in the resolution parametrization. The systematic uncertainty is evaluated by estimating the background with different *Met Model* predictions with a defaut set of parameters to predictions obtained with parameters deviated by $\pm\sigma$. Then we add statistical uncertainty and these systematic uncertainties in quadrature to obtain the total uncertainty.

3.3 Electroweak Backgrounds: $e + \gamma$ Events

Many electroweak processes with electrons in the final state have intrinsic $\not\!\!E_T$ and can fake the $\gamma\gamma + \not\!\!E_T$ final state. This occurs if an electron fakes a photon by loosing its track due to either tracking inefficiency or, more often, due to FSR and bremsstrahlung in the detector material in front of the COT [26]. If such an electron is accompanied by a real or fake photon, we can obtain a $\gamma\gamma$ signature with significant $\not\!\!E_T$. Examples of this kind of processes include inclusive $W\gamma \rightarrow e\nu\gamma$ production, $W+jet \rightarrow e\nu+jet$, $Z\gamma \rightarrow \tau\tau\gamma \rightarrow \tau e\nu\gamma$, $Z+jet \rightarrow \tau\tau+jet$, $Z \rightarrow \tau\tau \rightarrow e\nu e\nu$, etc. All these processes have one common signature: $e\gamma \rightarrow \gamma_{cand}\gamma$, i.e. one photon is faked by electron and the other photon candidate can be either a real or fake photon. We estimate all the above backgrounds by noticing that they all have the common $e\gamma$ final state and call all the processes mentioned above as the "$e\gamma$ background", and use this feature to obtain their combined contribution into $\gamma\gamma + \not\!\!E_T$ final state. Algorithmically we use the methods of Ref. [19].

To estimate the contribution from the electroweak backgrounds, we use the standard electroweak MC samples [28] and normalize to the production cross sections with a MC correlation factor. The Baur $W\gamma$ and $Z\gamma$ stntuples are used to evaluate contributions from both $W/Z + \gamma$ and $W/Z + \gamma\gamma$ events. The inclusive PYTHIA W and Z stntuples are used to obtain a contribution from $W + jet$, $Z \rightarrow e^+e^-/\tau^+\tau^-$, and $Z + jet$ events where both photon candidates are fakes. We consider all three leptonic decay modes of W and Z bosons. To avoid an overlap between Baur and PYTHIA, we filter out PYTHIA events where photons reconstructed in the detector are matched to HEPG level photons from either quark ISR or lepton FSR. After estimating this background, the expected $\not\!\!E_T$ *Significance* distributions of Electroweak Background is shown in Figure 8.

To minimize the dependence of our predictions on potentail Data-MC differences (trigger efficiencies, acceptance and ID efficiencies, k-factors, modeling of ISR/FSR, PDF uncertainties, luminosity uncertainties, etc.), we normalize our results to data. To achieve this goal, we select

$e\gamma + \not\!\!E_T$ events in data and MC. Then we take a ratio of $Data(e\gamma + \not\!\!E_T)/MC(e\gamma + \not\!\!E_T)$ to be a normalization factor in MC predictions for the $\gamma\gamma+\not\!\!E_T$ signature. While applying this normalization factor to predictions in the electron channels, we also take into account the Data-MC difference in the $e \to \gamma$ fake rate. The final normalization factors and relative contributions from $W/Z \to e$ channels, and the results for the $e + \gamma$ data samples are shown in Table 8.

The normalization factor uncertainty includes data and MC statistical uncertainties, uncertainty on the fake rate normalization factor and uncertainty associated with a contribution from fake $e + \gamma$ events into the $e + \gamma$ data sample and differences in MC modeling of the E/p distribution. The last uncertainty is estimated by comparing results for a default value of the E/p cut[2] ($0.8 < E/p < 1.2$) and a deviated value of the E/p cut ($E/p < 2.0$). The uncertainties include the MC statistical uncertianties and uncertainties on the normalization factors added in quadrature.

Cut	Number of Data (Total 3,617)	Data/MC	$(W/Z \to e)/(W/Z \to all)$ for Data	$(W/Z \to e)/(W/Z \to all)$ for MC
$MetSig > 3.0$	816	0.78±0.04	0.94	0.60
$MetSig > 4.0$	716	0.77±0.05	0.95	0.62
$MetSig > 5.0$	633	0.75±0.05	0.96	0.63

Table 8: The results for the $e + \gamma$ data samples, the final normalization factors (Data/MC) and relative contributions from $W/Z \to e$ channels. The MC predictions for $e+\gamma$ events are normalized to these numbers of data events.

3.4 Non-Collision Events

Non-Collision backgrounds to the $\gamma\gamma + \not\!\!E_T$ background come from PMT spikes, beam halo (B.H.) and cosmic rays (C.R.), where either a single or double photon-like signature comes from the non-collision source. Because these events do not originate from beam-beam interactions, they can be a source of significant spurious $\not\!\!E_T$. It was also shown in [23] that sources of spurious energy (other than C.R. or B.H.) in $\gamma\gamma$ events are negligible.

PMT spikes are rare and have a distinct signature (see Ref. [25]). The PMT asymmetry removes them very efficiently. Therefore, we do not explicitly evaluate this background and take the number of remaining PMT spikes backgrounds events to be zero. We next discuss B.H. and C.R.

3.4.1 Beam Halo Events

As discussed in Ref. [25] beam halo events fake the $\gamma\gamma + \not\!\!E_T$ final state when high energy muons, produced in beam-beam pipe interactions, interact the calorimeter. For geometric reasons these photon candidates are mostly located in the same wedge, mostly wedges 0 and 23 after. To predict the shape of the $\not\!\!E_T$ distribution after B.H. rejection cuts, we select a sample of $\gamma\gamma$ events using loose photon ID cuts (see Table 9) along with all other selection requirements (see Section 2) except that these events have neither vertex cuts ($|Z_{vertex}| < 60cm$) nor EMTiming cuts. There are 18 events in these samples shown in Figure 4. Next, we ues all 18 B.H. events to create a template for the $\not\!\!E_T$ and other kinematic distributions. The template is scaled by the corresponding numbers of

[2]The E/p cut is the only requirement that makes our electron ID different from photon ID.

remaining B.H. events (N_{BH}) based on the rejection power F_{BH} ($\sim 90\%, see Ref.$ [19]) to obtain the contributions due to this background. The scale factor is given by

$$N_{\rm BH} = N_{\rm BH}^{\gamma\gamma} \times (\frac{1}{F_{\rm BH}} - 1) \times F_{\rm cosmic} \quad (1)$$

where $N_{BH}^{\gamma\gamma}$ is the number of observed B.H. events and F_{cosmic} ($\sim 67\%$) is cosmic rejection power.

The uncertainties on B.H estimation are mostly dominated by statistical uncertainty on the number of identified B.H. events. The other source of uncertainty, though much smaller, is the uncertainty on fraction of B.H. events that pass EMTiming cuts.

Cuts	Loose control sample ID
detector	CEM
corrected E_T	$\geq$ 13 GeV
CES fiduciality	$\lvert X_{\rm CES}\rvert \leq 21$ cm 9 cm $\leq \lvert Z_{CES}\rvert \leq 230$ cm
average CES χ^2	$\leq$20
Had/Em	$\leq$0.125
corrected CalIso0.4	$\leq 0.15\times E_T$ if $E_T<20$ GeV or $\leq 3.0+0.02\times(E_T - 20)$
TrkIso0.4	≤ 5
$N3D$ tracks in cluster	≤ 1
track P_T if $N3D = 0$	$\leq 0.25\times E_T$
E_T of 2^{nd} CES cluster (wire and strip)	no cut

Table 9: Summary of the standard loose photon ID cuts. The control sample is used to estimate background.

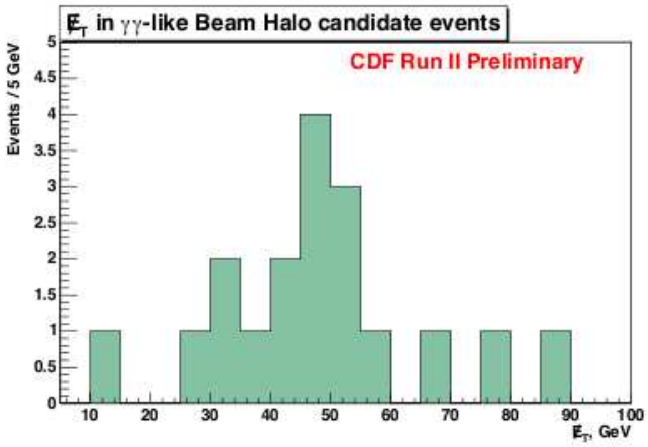

Figure 4: The $\not\!\!E_T$ distribution in observed $\gamma\gamma$-like beam halo events.

3.4.2 Cosmic Ray Events

Cosmic ray events fake the $\gamma\gamma + \not\!\!E_T$ signature as the muon traverses the magnet, or by catastrophic interaction with the EM calorimeter. We use the muon system to suppress this type of background in data before run 190851 (see Table 6). We rely on the EMTiming system to remove the contamination due to cosmic ray after run 190851. Our method to evaluate the contribution due to cosmic rays faking $\gamma\gamma + \not\!\!E_T$ signature is based on the EMTiming system which allows for unambiguous identification of cosmic ray events using the timing window [25,90] ns and extrapolation into the signal window. We first determine the rate of $\gamma\gamma$-like cosmic events and the rejection power of a cut on the number of trackless muon stubs in "new" data after run 190851, and then extrapolate these results on the "old" data before run 190851.

We begin with selecting $\gamma\gamma$-like cosmic ray events which is used to determine the efficiency of a cut on trackless muon stubs, the efficiency of a cut on $\Delta T_{\gamma\gamma}$ between arrival time of two photons, and to obtain a template for the $\not\!\!E_T$ and other kinematic distributions in cosmic events. To increase statistics, the following requirements are loosened: loose photon ID cuts (Table 9), at least one of the photon candidate must have $T_\gamma > 25$ ns or $|\Delta T(\gamma_1 - \gamma_2)| > 8$ ns, and events are allowed to fail our vertex cut ($|Z_{vx}| < 60$ cm). We select 26 $\gamma\gamma$-like cosmic ray events. The $\not\!\!E_T$ distributions for these events are shown in Figure 5.

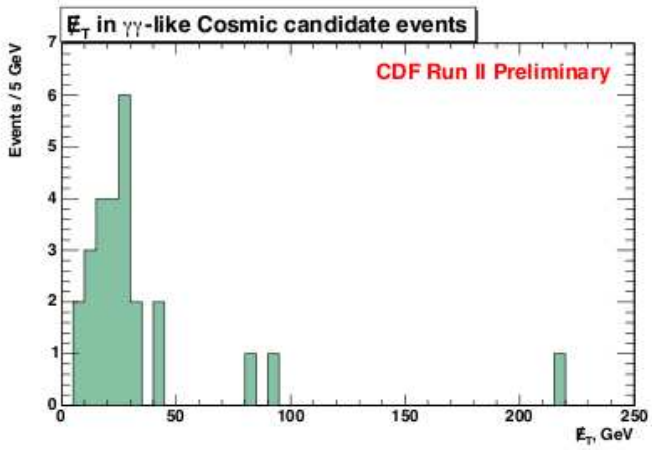

Figure 5: The $\not\!\!E_T$ distribution in observed $\gamma\gamma$-like cosmic events.

The strategy to evaluate the number of remaining cosmic events in data after run 190851 is based on the fact that the cosmics arrival time is independent of the collision time. Therefore, we simply count the number of events where at least one of two photons have the arrival time in the range 30 ns$< T_\gamma <$120 ns. Then we require these events to pass $|T_\gamma| < 4 \times 1.665$ ns cut. Finally, a cut on $\Delta T_{\gamma\gamma}$ between arrival time of two photons is applied.

To evaluate the number of the remaining cosmic events in date before run 190851, we use the observed number of cosmic events in the data with the EMTiming system and assume that the cosmics rate per bunch crossing is the same in both samples. This makes our final estimate for the number of the remaining cosmic ray events: $N_{cosmic} = N_2(1 - f_{muon}) + N_2(1 - f_{stub})$, where f_{muon} is a fraction of data with good muon system, and f_{stub} is a rejection power of a cut on trackless muon stub, N_2 is a number of cosmic events in "old" data (before run 190851), and N_1 is a number of cosmic events in "new" data (after run 190851). Then, combining our predictions for "old" and "new" data, we predict the number of remaining cosmic ray events.

The uncertainties are mostly dominated by statistical uncertaintiy on the number of identified cosmics events. Other sources of uncertainty are uncertainties on efficiency of no-stub and ΔT cuts.

3.5 Fake $\not\!\!E_T$ from Picking the Wrong Vertex

A source of QCD background that is unaccounted for by the *Met Model*, is di-photon events with a wrong choice of the primary interaction vertex. This occurs when a $\gamma\gamma$ pair is produced by one interaction and, for example, a pair of jets is produced at another vertex producing the highest $\sum$P$_T$ vertex. Hard scattering processes involving jets have, in general, more tracks compared to interactions where no jets are produced. Therefore, if one vertex produces jets and the other one gives $\gamma\gamma$ pair, then it is very likely that the former vertex will be picked as a primary one. Wrong vertex results in E_T mis-measurement and can give fake $\not\!\!E_T$. Although this mis-measurement is small in most occasions, sometimes it can overlap with already mis-measured jets and produce significant $\not\!\!E_T$.

To obtain a prediction for this background contribution we use PYTHIA $\gamma\gamma$ events where the hard interaction does not produce a vertex, and the primary vertex is due to an overlapping Minimum Bias interaction. First, we determine the fraction of such events in data. We have two methods to get this fraction. The first method is based on the difference between the photon and vertex timing, $\Delta T_\gamma - T_{vx}$, in $\gamma\gamma$ candidate events with only one reconstructed vertex. The second method to obtain this fraction is based on MC and Zero Bias data. The second method gives us a 4.8±0.4% fraction of "no vertex" events in the $\gamma\gamma$ sample, which agrees very well with 5±1% obtained from the first method. We take 4.8% as the default value, and the difference between these two estimates is taken to be a systematic uncertainty. The fraction is used to normalize our MC template of "no vertex" $\gamma\gamma$ events to data. The expected $\not\!\!E_T$ *Significance* distribution of the wrong vertex background is shown in Figure 6.

The uncertainty on wrong vertex background estimation comes from a fraction of diphoton events without vertex.

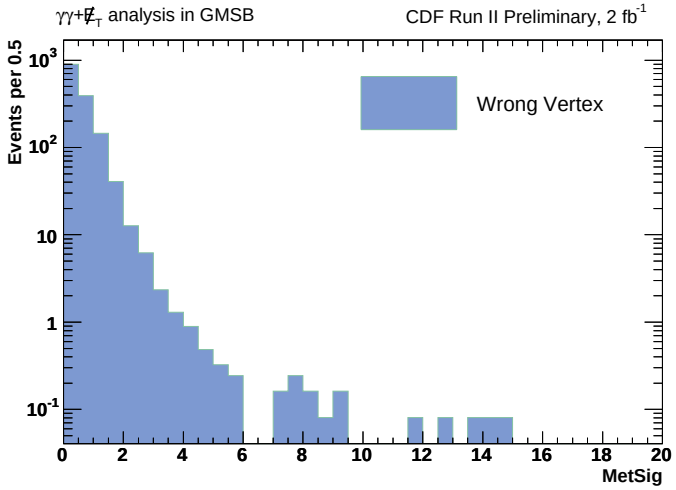

Figure 6: The wrong vertex background prediction of $\not\!\!E_T$ *Significance* distribution for the pre-sample.

3.6 Tri-Photon Events with a Lost Photon

There is a second class of QCD events whose contribution into the $\gamma\gamma+\not\!\!E_T$ signature is not estimated by the *Met Model*. These events are *tri-photon* events[3] with a lost photon. The cross section of this process is very small. However, the probability to lose a photon in the calorimeter cracks is on the order of ∼10% or more[4], so that the probability to lose one of the photon candidates in a *tri-photon* event can be ∼30% or larger. These events will look like perfect $\gamma\gamma + \not\!\!E_T$ events for the *Met Model* because it only accounts for fake $\not\!\!E_T$ due to fluctuations in energy measurements.

To estimate this background, we use "cdfpstn:gx0s1g" PYTHIA $\gamma\gamma$ sample with large statistics. We start by selecting reconstructed tri-photon candidate events ($E_T^{\gamma 1,2,3}$ >13 GeV) in both MC and data. This number gives us a MC-to-Data normalization factor: $N_{Data}^{\gamma\gamma\gamma}/N_{MC}^{\gamma\gamma\gamma}$, where $N_{Data}^{\gamma\gamma\gamma}$ is the number of reconstructed PYTHIA tri-photon events, $N_{MC}^{\gamma\gamma\gamma}$ is the number of reconstructed data tri-photon events. Then we select PYTHIA tri-photon events at the generator level, apply all of the analysis cuts to these events, and multiply the result by the the scale factor given above: $N_{MC}^{\gamma\gamma\gamma}/N_{Data}^{\gamma\gamma\gamma} * N_{lost\ \gamma}^{\gamma\gamma\gamma}$, where $N_{lost\ \gamma}^{\gamma\gamma\gamma}$ is the number of PYTHIA tri-photon events with lost photon.

The systematic uncertainties on this background prediction include the following source: 1) uncertainty on the scale factor; 2) uncertainty due to difference in the unclustered energy parameterization; 3) jet energy scale uncertainty. The expected $\not\!\!E_T$ *Significance* distribution of the tri-photon background is shown in Figure 7.

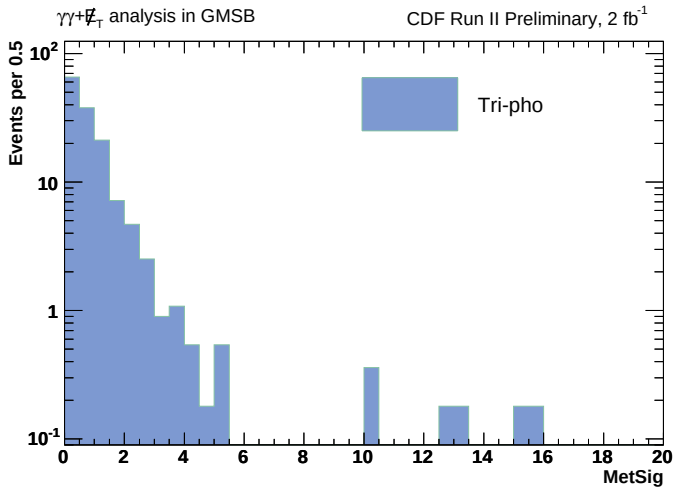

Figure 7: The tri-photon background prediction of $\not\!\!E_T$ *Significance* distribution for the pre-sample.

3.7 Background Summary

After estimating all the backgrounds, the expected $\not\!\!E_T$ *Significance* distributions of QCD (wrong vertex, tri-pho predictions are included), electroweak, non-collision (beam halo and cosmic rays) and all combined for the pre-sample are shown in Figure 8

[3]One of the photon candidates can be a fake

[4]This is an educated guess, and it is based on a fact that the CEM ϕ-cracks alone account for ∼8% of the CEM area

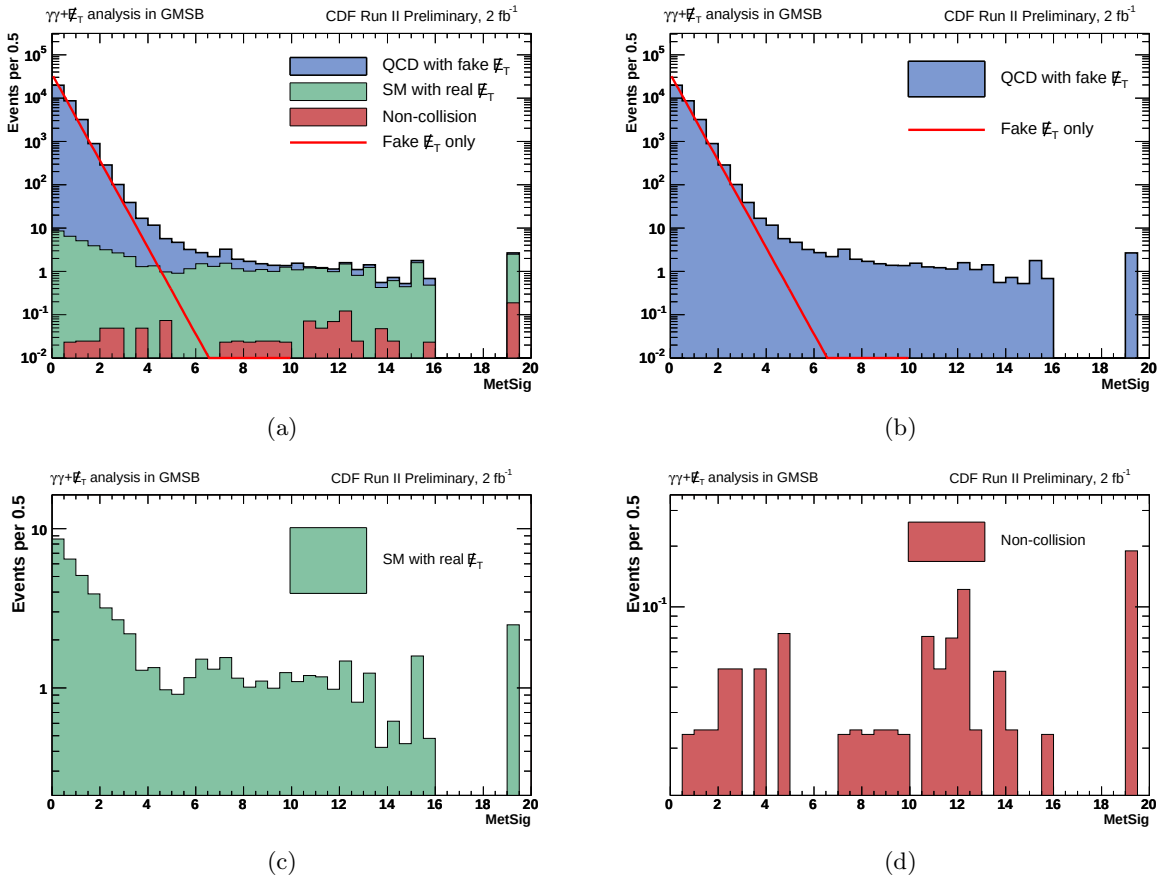

Figure 8: The background predictions for the pre-sample. (a) shows total predictions for all the backgrounds along with the perfect prediction of fake $\not\!\!E_T$ only. QCD backgrounds include tri-pho and wrong vertex backgrounds along with the perfect predicion of fake $\not\!\!E_T$ only in (b). (c) shows the prediction for electroweak background. Non-collision backgrounds include beam halo and cosmic rays in (d).

4 Accepances on GMSB Model

In this section we describe the MC simulation of the GMSB model, and how we estimate our signal acceptance. We use the PYTHIA event generator. For the purpose of this analysis we consider a GMSB model with the following parameters fixed on the minimal-GMSB Snowmass slope constraint (SPS 8) that is commonly used [7, 9]:

$$N = 1, \quad M_m/\Lambda = 2, \quad \tan\beta = 15, \quad \mu > 0.$$

This reduces above six free parameters to two: the $\tilde{\chi}_1^0$ mass and lifetime We use *cdfSim* of *cdfsoft* release 6.1.4 [29, 12] with the default settings, modified for the simulation of the EMTiming system (see App. B in Ref. [30]). We simulate the full GMSB model with the setting MSEL=39 with the masses calculated with ISASUGRA [31]. We use the detector calibrations of runnumber 191636 for all MC samples. Each sample contains 100,000 events which yields a statistical uncertainty of $\sim 1\%$ if the probability for signal events to pass our cuts is $\sim 9\%$. For our analysis we only consider $\tilde{\chi}_1^0$'s lifetimes up to 2 ns since *cdfSim* does not simulate CES-χ_2 correctly for higher lifetimes [30]. Also the next generation delayed photon analysis will deal with high lifetimes.

The total event accepance, $A_{SignalMC}$, is used when calculating the cross section limits, and is quantitatively defined by:

$$A_{Signal\ MC}(\%) = \frac{N_{\text{events}}^{\text{passing all cuts}}}{N_{\text{events}}^{\text{total produced}}}. \tag{2}$$

The breakdown of events after passing each of the selection cuts for an example GMSB point at $m(\tilde{\chi}_1^0) = 140$ GeV and $\tau(\tilde{\chi}_1^0) = 0$ ns is shown in Table 10. For completeness we have included the results for the final event selection, determined in Section 6. We have ignored the muon stub cuts and different analysis for the early data for now as it produces only a $\sim 0.5\%$ difference.

Requirement	Events passed	$A_{\text{Signal MC}}$ (%) ($m(\tilde{\chi}_1^0) = 140$ GeV and $\tau(\tilde{\chi}_1^0) = 0$ ns)
Sample events	100000	100.00
Two EM Objects and $\lvert z_{vertex}\rvert < 60\ cm$	92010	92.0
Photon fiducial & Standard ID cuts	14190	14.2
Phoenix Rejection & PMT cuts	13785	13.8
Beam Halo and Cosmic Rejection cuts	13781	13.8
$\not\!\!E_T\ Significance$>3	10367	10.4
H_T>200 GeV	9802	9.8
$\Delta\phi(\gamma_1,\gamma_2)<\pi - 0.15$	9217	9.2

Table 10: Summary of the event reduction for a GMSB example point in the $\gamma\gamma$+$\not\!\!E_T$ final state. We have included the final, optimized cuts for completeness.

5 Estimation of the Systematic Uncertainties

In order to estimate the sensitivity of the search we calculate the expected 95% C.L. cross section limits, which involves the uncertainties in the luminosity, background and acceptance. The systematic uncertainty on the luminosity is taken to be 6% with major contributions from uncertainties on the CLC acceptance from the precision of the detector simulation and the event generator [32]. The systematic uncertainty on the background in the signal region is determined from our understanding of both the collision and non-collision sources, as described in Section 3. The background uncertainty is evaluated for every set of cuts in the optimization procedure. The acceptance and cross section uncertainties are estimated in the subsections below. The results are summarized in Table 11 for an example GMSB point of $m(\tilde{\chi}_1^0) = 140$ GeV and $\tau(\tilde{\chi}_1^0) = 0$ ns. All uncertainties are consistent with the GMSB diphoton analysis in Ref. [7] unless otherwise noted. We take the systematic uncertainty to be constant for all masses.

Factor	Relative Systematic Uncertainty (%)
Acceptance:	
Diphoton ID and Isolation	5.4
ISR/FSR	3.9
JES	1.6
$\not\!\!E_T$ *Significance* parameterizations	0.7
PDFs	0.4
Pile-up effect on $\not\!\!E_T$ *Significance*	x.x
Total	x.x
Cross section:	
PDF	7.6
Renormalization scale (Q^2)	2.6
Total	8.0

Table 11: Summary of the systematic uncertainties on the acceptance and production cross section for an example GMSB point at $m(\tilde{\chi}_1^0) = 140$ GeV and $\tau(\tilde{\chi}_1^0) = 0$ ns.

5.1 Acceptance Errors

There are a number of effects that can cause our estimate of the acceptance to be incorrect. We identify them here, by order of decreasing magnitude, and explain how they are estimated.

5.1.1 Photon ID and Isolation Efficiencies

The photon ID and Isolation variables are imperfectly modeled in the *cdfSim*. This has been studied in detail eslewhere. We take a systematic uncertainty of 1.8% for the photon ID and 2.0% for isolation efficiencies as described in Ref. [33, 34] in quadrature for a total of 2.7% uncertainty per photon. Since there are two photons, we take the total systematic uncertainty to be $2\times2.7\% = 5.4\%$. This represents an improvement over the 202 pb^{-1} result due to improved understanding of the detector.

5.1.2 ISR/FSR (Initial and Final State Radiation)

Initial state radiation (ISR) caused by a gluon radiating from an incoming parton or final state radiation (FSR) from an outgoing jet can both make the E_T spectrum of the final state particles softer than expected without radiation. This can cause the photon, the jet or the $\not\!\!E_T$ to be systematically more likely to pass the kinematic requirements. The effect carries a non-negligible theoretical uncertainty and is estimated using the standard CDF procedure by varying the Sudakov parameters as described in [35]. Doing so we find a variation in the acceptance, taken to be the systematic uncertainty, of 3.9%.

5.1.3 JES (Jet Energy Scale)

Since we allow jets with a corrected E_T of > 15 GeV in our set of events we have studied the change in acceptance if the jet energy is mismeasured. The following effects are taken into account: relative jet energy, underlying event, multiple interaction, absolute energy scale, out-of-cone and splash-out. The standard procedure at CDF [36] varies each correction factor independently by $\pm 1\sigma$. The resulting variation in the acceptance is $\pm 1.6\%$.

5.1.4 $\not\!\!E_T$ *Significance* parameterization and calibration

The $\not\!\!E_T$ *Significance* calibrations and unclustered-energy parameterizations are slightly different for data and MC (See Fig. 10 and 16 in Ref. [19]). To estimate the magnitude of this uncertainty on the acceptance, we compare the acceptance using the most different sets and find the uncertainty on the acceptance to be 0.7%.

5.1.5 PDFs (Structure Functions)

In an event where proton and antiproton bunches collide it is mostly a single subparticle of the (anti-)proton, a parton (quark or gluon), that participates in the hard collision and produces a high center-of-mass energy event. The momentum fraction, described by parton distribution function (PDFs), that is carried by each of the partons in the proton or antiproton is not perfectly understood. If affects both the rate at which a process happens (the production cross section) and the kinematics of the outgoing final state particles (the acceptance of the event selection criteria).

For each simulated event the MC generator calculates the momentum fraction of the colliding parton using a standardized "PDF-set" by the `CTEQ` collaboration (`CTEQ-5L`) [37]. As only the newer PDF-set version `CTEQ-6M` contains 90% confidence intervals for each eigenvector, the total uncertainty is estimated using a standard procedure by reweighting the parton momenta of the original `CTEQ-5L` set and varying the PDFs using the uncertainties from `CTEQ-6M` as described in Ref. [37]. For the example GMSB point we get a relative uncertainty of $+0.3\%$ -0.4% [38] on the acceptance. We take the larger value to estimate the uncertainty conservatively.

5.1.6 Pile-Up effects on $\not\!\!E_T$ *Significance*

Since there is a substantial pile-up of E_T in events with multiple collisions, false jets may be detected at low jet E_T, while at higher jet energies the extra pileup energy must also be accounted for. This procedure in progress now.

5.2 Production Cross Section Errors

5.2.1 PDFs (Structure Functions)

Using the same methods in subsection 5.1.5, but considering the total production cross section calculation, for the example GMSB point we get a relative uncertainty of $+7.6\%$ -7.3% on the cross section. We take the larger value to estimate the uncertainty conservatively. This uncertianty is a little bit bigger than what we had in the delayed photon analysis ($\sim$ 5.9% for $\tilde{\chi}_1^0$ mass=100 GeV) since our example point uses a heavier mass.

5.2.2 Q^2 (Renormalization Scale)

While the dominant GMSB production mechanisms are via electroweak processes (see Fig. 1), the probability that QCD processes occur via gluon emission and higher-order loops depend sensitively on the energy scale at which the process happens. In PYTHIA [12] events are generated using a fixed renormalized (q^2) scale of $\hat{s}$. However, the NLO cross section, which is calculated with PROSPINO2 [39], varies as a function of the renormalization scale. The variation of the NLO production cross section observed by changing the scale from $0.25 \cdot q^2$ to $4 \cdot q^2$ is calculated to be 2.6% for the example GMSB point.

We use the 18% for the total systematic uncertianty from the 202 pb^{-1} for now to be conservative until our final estimates are done.

6 Optimization and Expected Limits

Now that the background is estimated and the signal acceptance is available for a given set of cuts, along with their uncertainties, an optimization procedure can be readily employed to find the optimal cuts before unblinding the signal region. We optimize for the following cuts[5]: $\not\!\!E_T$ $Significance$, H_T[6], and $\Delta\phi(\gamma_1, \gamma_2)$. We optimize for all requirements simultaneously at each GMSB parameter point. Once we have the optimal values at each point we then decide for a set of cuts that we deem robust enough to be applied throughout the parameter space for simplicity.

We choose to optimize for $\not\!\!E_T$ $Significance$, H_T, and $\Delta\phi(\gamma_1, \gamma_2)$ cuts for following reasons:

- $\not\!\!E_T$ $Significance$ cut:
  As described in Section 3, this cut gets rid of most of the QCD background with fake $\not\!\!E_T$.

- H_T cut:
  In GMSB production heavy gaugino pari-prodcution dominates, which decays to high E_T, light final state particles via cascade decays. GMSB signal has lots of H_T compared to SM backgrounds, which is dominated by QCD and Electroweak backgrounds which do not have lots of high E_T objects.

- $\Delta\phi(\gamma_1, \gamma_2)$:
  Electroweak backgrounds with large H_T are typically a high E_T photon recoiling against $W \to e\nu$, which means the gauge boson decay is highly boosted. Thus, the two photon candidates in the final state are mostly back to back. Also the high E_T diphoton with large H_T from QCD background are mostly back to back with fake $\not\!\!E_T$ or wrong vertex. The $\Delta\phi(\gamma_1, \gamma_2)$ cut gets rid of these back to back photons.

By estimating our sensitivity using the 95% C.L. expected cross section limits on GMSB models in the no-signal assumption, we find the optimal set of cuts before unblinding the signal region. We use the standard CDF cross section limit calculator [40] to calculate the limits, taking into account the predicted number of background events, the acceptance, the luminosity and their systematic uncertainties (see Section 5). We take

$$\sigma_{95}^{\rm exp} = \sum_{N_{obs}=0}^{\infty} \sigma_{95}^{obs}({\rm cut}) \times {\rm Prob}(N_{obs}, N_{exp} = \mu) \quad (3)$$

$${\rm RMS}^2 = \sum_{N_{obs}=0}^{\infty} (\sigma_{95}^{obs}({\rm cut}) - \sigma_{95}^{\rm exp})^2 \times {\rm Prob}(N_{obs}, N_{exp} = \mu) \quad (4)$$

where N_{obs} is the number of observed events in the pseudoexperiment, μ is the mean of the number of expected events as a function of the cuts and σ_{95}^{obs} denotes the cross section limit if N_{obs} were observed. Each are a function of the cut choices. The expected cross section limit is then a function of the these cuts.

For each GMSB point there is a minimum expected cross section limit for a set of optimal cuts. As an illustration of the optimization, Figures 9-(a), (c), and (e) show the expected cross section limit as a function of a cut after keeping all other cuts fixed at the already optimized values. Indicated in green is the 8.0% uncertainty-band on the production cross section. In yellow we show the expected variation in the expected cross section limit using the data in Table 12 and the RMS definition in Eq. 4. We decided to use a single set of cuts before we open the box based with the expectation that they will yield the largest expected exclusion region. We

[5]Many ohter cuts were considered, including $\not\!\!E_T$, $\Delta\phi(\gamma, \not\!\!E_T)$, E_T^{γ}, etc., but these yield negligible gain and add additional systematics

[6]Sum of E_T of all EM objects such as photons, jets with $E_T > 15$ GeV and $|\eta| < 2.4$ and $\not\!\!E_T$

chose: $\not\!\!E_T$ $Significance$>3, H_T>200 GeV, $\Delta\phi(\gamma_1,\gamma_2)<\pi-0.15$ rad. With thess cuts we predict 0.62±0.29 background events with 0.39±0.18 from SM electroweak with real $\not\!\!E_T$, 0.049±0.050 from non-collision, and 0.10±0.22 from QCD with fake $\not\!\!E_T$ listed in Table 13.

Table 14 shows the expcted cross section limits, acceptance and production cross section of each GMSB point simulated, along with the predicted background.

Figures 9-(b), (d), and (f) show the distributions of each optimization variable normalized to the number of expected events, after applying all optimized cuts. We compare the background distribution before unblinding the signal region and the expected signal in the signal region for an example GMSB point at $m(\tilde{\chi}_1^0) = 140$ GeV and $\tau(\tilde{\chi}_1^0) = 0$ ns. Taking into account the errors we expect an acceptance of (9.21±1.66)%. Next we unblind the signal region and set limits on GMSB models.

We note that we do not do a separate optimization for non-zero lifetimes. Rather we simply estimate the sensitivity of our analysis to these scenarios. The expected results are given in Table 14.

N_{obs}	$\sigma_{obs}(N)$ (fb)	Probability
0	16.9	0.538
1	24.6	0.334
2	32.9	0.103
3	41.5	0.021
4	50.0	0.003

Table 12: The 95% C.L. cross section limit as a function of the hypothetically observed number of events and the Poisson probability for this number of events based on the background expectation of 0.62 event. The expected limit and its variation are calculated as shown in [40] with Eqs. 3 and 4 using the optimized background expectation, acceptance and production cross section at an example GMSB point of m($\tilde{\chi}_1^0$)=140 GeV/c^2 and $\tau(\tilde{\chi}_1^0)$=0 ns. With these numbers we get an expected cross section limit of 21.8 fb and an RMS on the limit of 6.4 fb.

Backgrounds	Estimations
Baur $W(e)+\gamma$	0.049±0.049
Baur $W(\mu)+\gamma$	0.00±0.047
Baur $W(\tau)+\gamma$	0.14±0.082
Baur $Z(e)+\gamma$	0.006±0.004
Baur $Z(\mu)+\gamma$	0.079±0.015
Baur $Z(\tau)+\gamma$	0.052±0.012
Pythia $W(l)$ no ISR/FSR	0.0±0.086
Pythia $Z(l)$ no ISR/FSR	0.0±0.026
Pythia $t\bar{t}$ (incl.)	0.046±0.009 (stat. only down to here)
QCD	0.10±0.10±0.00
Beam Halo	0.0±0.023±0.010
Cosmic Rays	0.049±0.035±0.026
Tri-Pho	0.00±0.180±0.035
Wrong Vertex	0.00±0.081±0.008

Backgrounds	Estimations
Electroweak	0.39±0.14±0.11
QCD	0.10±0.10±0.00
Non-Collision	0.049±0.042±0.028
Tri-Pho	0.00±0.180±0.035
Wrong Vertex	0.00±0.081±0.008
Total	0.62±0.26±0.12

Table 13: Summary of the background estimations after optimization. Top table shows each components of backgrounds. Bottom lists their combined predictions.

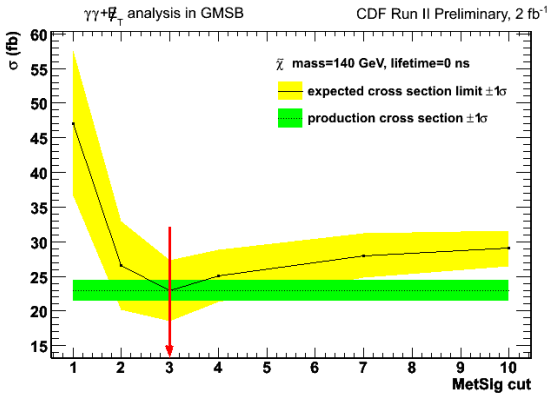

(a)

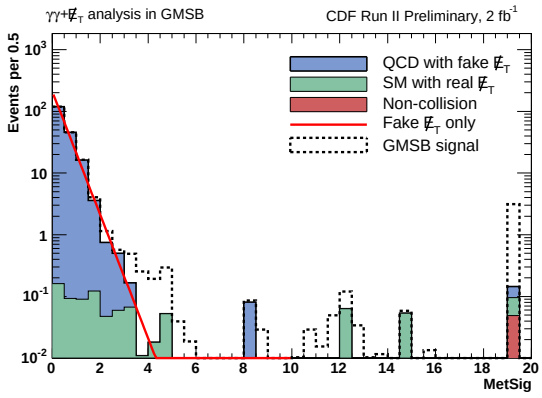

(b)

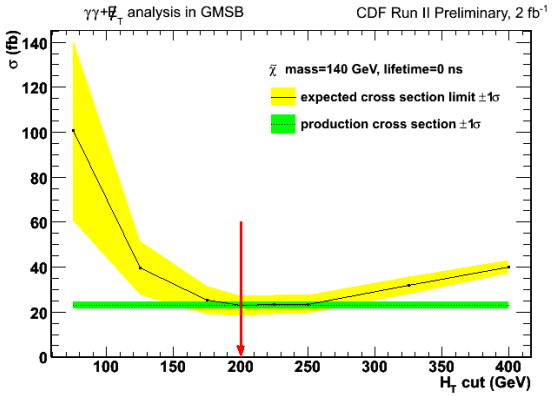

(c)

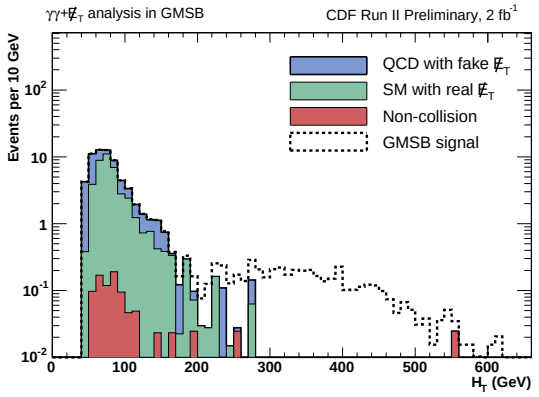

(d)

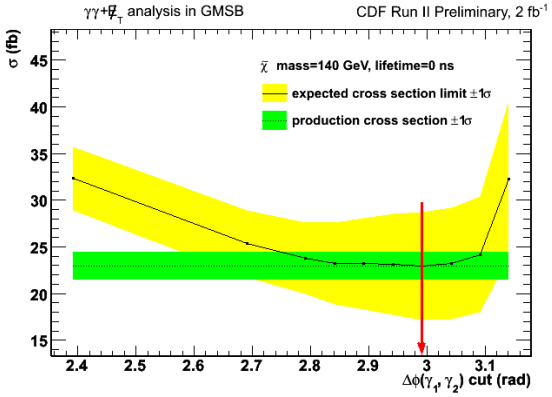

(e)

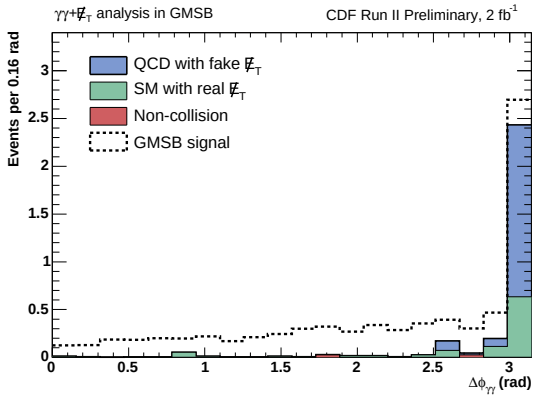

(f)

Figure 9: The expected 95% C.L. cross section limit as a function of the $\not\!\!E_T$ *Significance* (a), H_T (c), and $\Delta\phi(\gamma_1, \gamma_2)$ (e) requirement for a GMSB example point ($m(\tilde{\chi}_1^0) = 140$ GeV and $\tau(\tilde{\chi}_1^0) = 0$ ns). The optimal point is where the expected cross section is minimized. Indicated in green is the 8.0% uncertainty-band for the production cross section (see Table 11) and in yellow is the RMS (See Eqn. 4). The N-1 predicted kinematic distributions after the optimized requirements are shown in Figure (b), (d), and (f).

$m_{\tilde{\chi}}$ (GeV/c^2)	$\tau_{\tilde{\chi}}$ (ns)	Acceptance (%)	Background	$\sigma_{95}^{\rm exp}$ (fb)	$\sigma_{95}^{\rm obs}$ (fb)	$\sigma_{95}^{\rm prod}$ (fb)
70	0	2.40±0.43		87.71	98.62	
70	1	2.18±0.39		96.56	108.6	999.9
70	2	1.60±0.29		132.3	148.8	
80	0	4.88±0.88		43.36	48.65	
80	1	4.37±0.79		48.42	54.33	524.6
80	2	3.32±0.60		63.74	71.52	
90	0	6.08±1.10		34.80	39.05	
90	1	5.20±0.94		40.70	45.66	286.8
90	2	4.10±0.74		51.61	57.91	
100	0	7.93±1.43	0.62±0.29	26.68	29.94	
100	1	7.53±1.36	(1 observed)	28.10	31.53	169.0
100	2	5.80±1.04	EWK:	36.38	40.81	
110	0	8.33±1.50	0.39±0.18	25.37	28.50	99.47
110	1	8.30±1.49	Non-Collision:	25.43	28.52	
120	0	8.48±1.53	0.049±0.050	24.95	28.00	
120	2	6.63±1.19	QCD:	31.83	35.70	58.38
130	0	9.25±1.66	0.18±0.22	22.81	25.59	
130	1	9.47±1.70		22.28	24.99	36.23
130	2	7.00±1.26		30.20	33.92	
140	0	9.21±1.66		22.96	25.78	
140	1	9.26±1.67		22.85	25.64	22.97
140	2	7.15±1.29		29.59	33.21	
150	0	9.35±1.68		22.57	25.31	14.54

Table 14: The acceptance and expected cross section limits for various simulated GMSB points for the final selection requirements. For completeness, we have included both the expected and observed number of events and cross section limits from Section 6. Note we use the same analysis for lifetimes 0, 1 and 2 ns.

7 Data, Cross Section Limits and Final Results

In this section we unblind the signal region, set cross section limits and show the exclusion regions in neutralino mass and lifetime space for GMSB models.

7.1 The Data and Cross Section Limits

After all optimal cuts we open the box and observed one event, consistent with the expected 0.62±0.29 events. This event appears to be from the prompt collision background that is expected to dominate.

Figure 10 shows the kinematic distributions for the background and signal expectations along with the data. There is no distribution that hints at an excess and the data appears to be well modeled by the background precdiction alone.

7.2 Event 201674, 3054218

Since this event passes all optimal cuts we study it for evidence that it comes from GMSB, SM collision, or non-collision (beam halo or cosmic ray) background sources. Table 15 compares the event properties to the selection requirements, and Fig. 11 shows the CDF event displays in both the $r-\phi$ and the $\eta-\phi$ planes for the event.

7.3 The GMSB Exclusion Region

Fig. 12 shows the predicted and observed cross section limits along with the NLO production cross section (see Table 11) as a function of $\tilde{\chi}_1^0$ lifetime at a mass of 140 GeV/c^2 and as a function of mass at a lifetime of 0 ns. Indicated in green is the 8.0% uncertainty-band on the production cross section. In yellow we show the expected variation in the expected cross section limit using the data in Table 12 in Section 6 and the RMS definition in Eq. 4. Since the number of observed events is above expectations, the observed limits are slightly worse than the expected limits. The $\tilde{\chi}_1^0$ mass reach, based on the predicted (observed) number of events is 140 GeV/c^2 (138 GeV/c^2), at a lifetime of 0 and 1 ns. We do not consider lifetimes about 2 ns as most of the parameter space in high lifetimes there should be excluded by searches in single delayed photon analysis [6, 16]. Fig. 13 shows the 95% C.L. NLO exclusion region as a function of mass and lifetime of $\tilde{\chi}_1^0$ using the fixed choice of cuts from the optimization both for the predicted and observed number of background events. These limits extend the delayed photon results to bothe masses and lifetimes, at large masses, reaches well beyond those of DØ searches [18] and are currently the world's best.

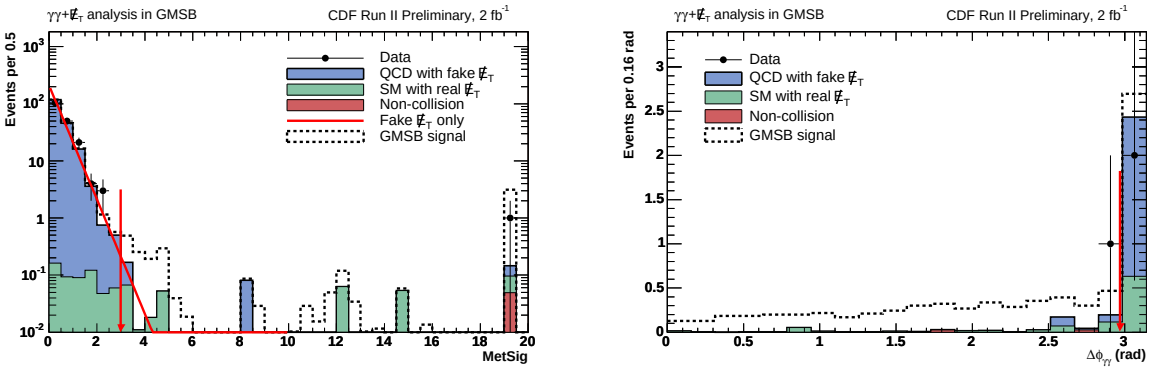

(a) (b)

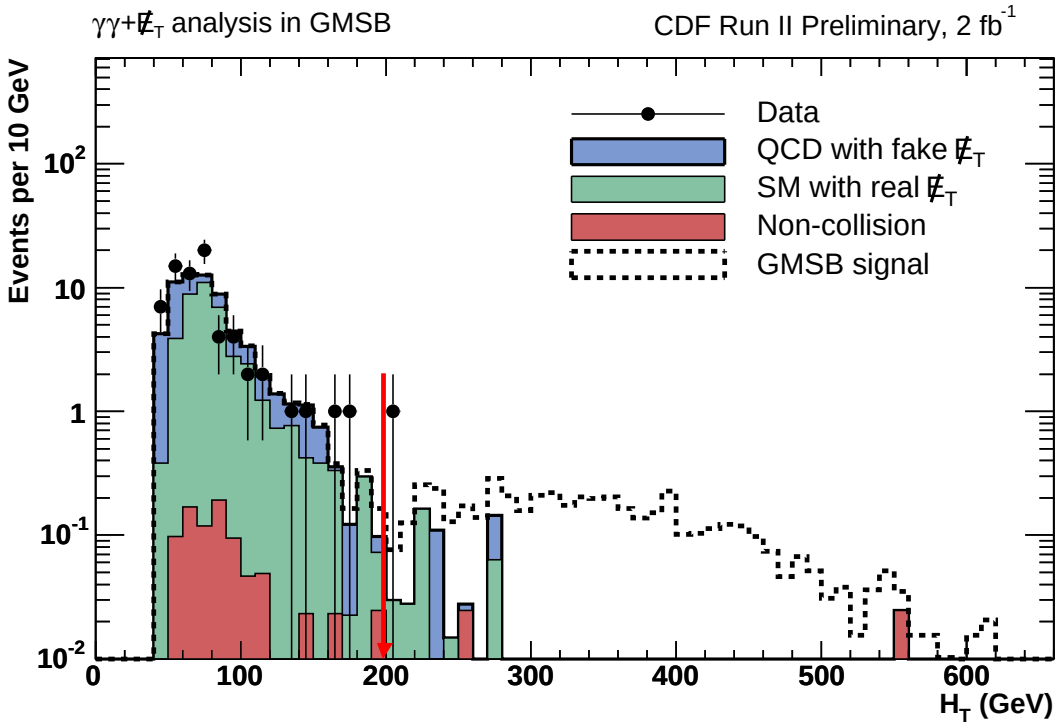

(c)

Figure 10: The same N-1 plots as Figure 9, but including the data. Each variable is plotted through the whole region while holding other variables at optimal cuts. There is no evidence for new physics.

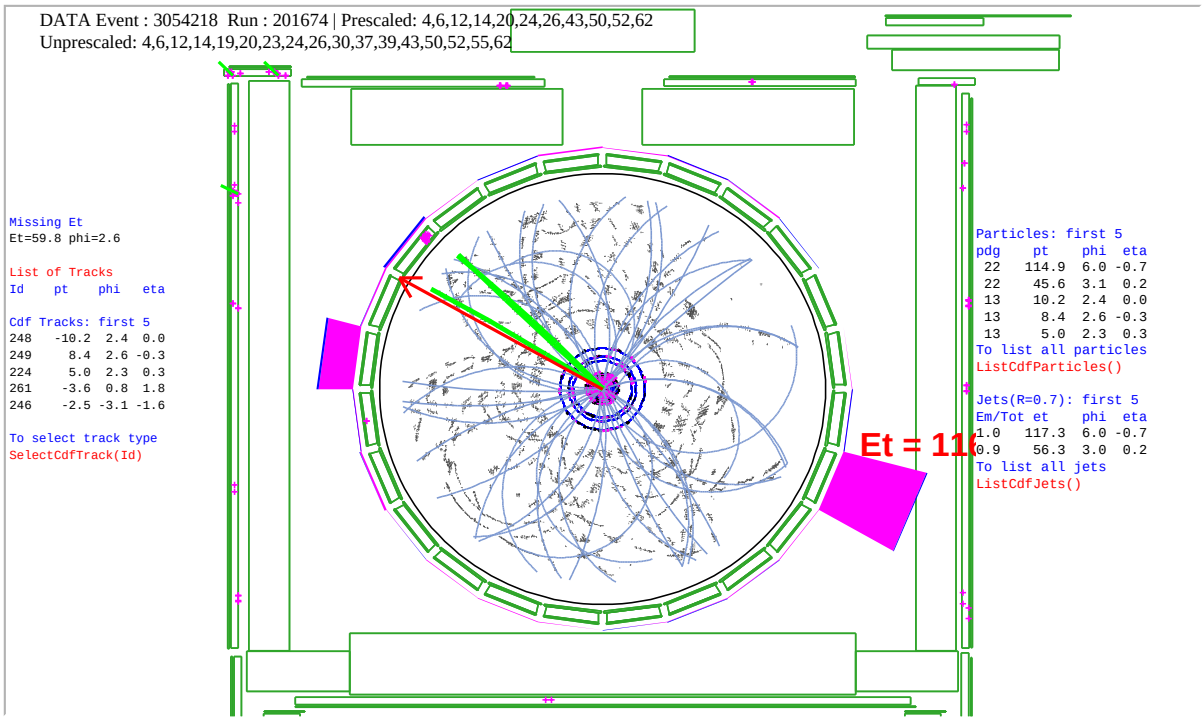

(a)

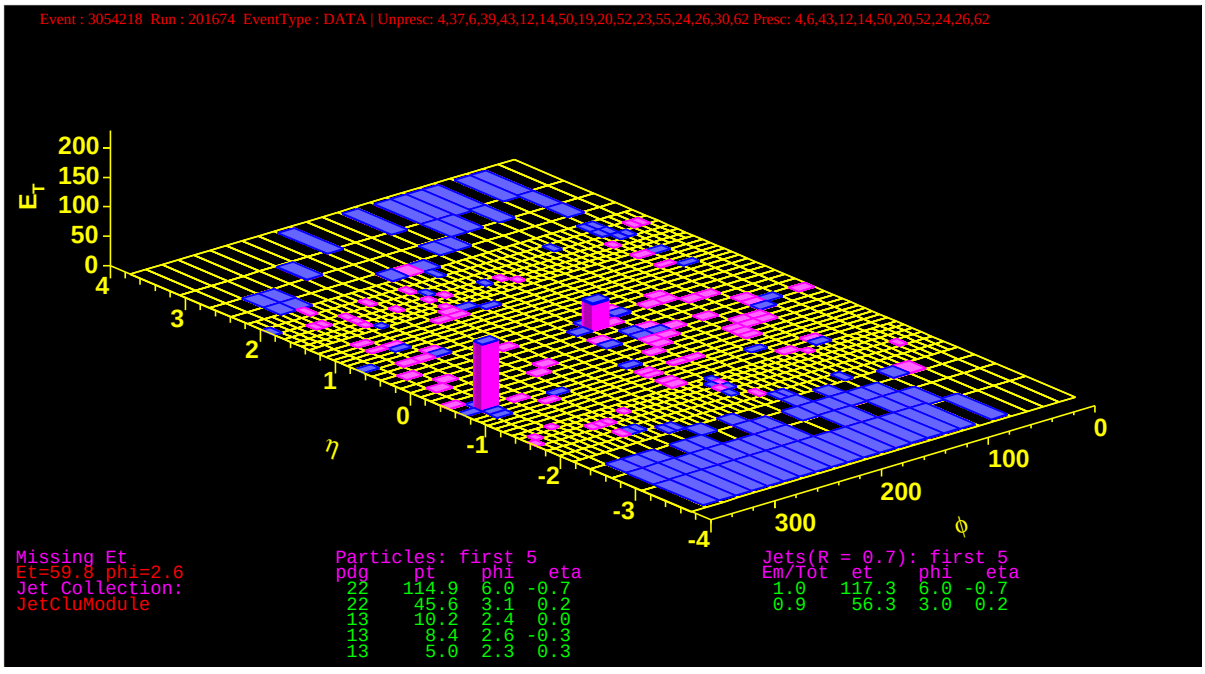

(b)

Figure 11: A view in the $r - \phi$ plane along the beam direction and the calorimeter towers in the $\eta - \phi$ plane for event 201674, 3054218.

Requirement	Value
Photon 1	
$E_T > 30$ GeV	106.5 GeV
$\lvert X_{\rm CES}\rvert < 21$ cm	-11.85 cm
9 cm$< \lvert Z_{\rm CES}\rvert < 230$ cm	-135.53 cm
Central	$\eta_{\rm det} = -0.681$ $\phi = 5.95$
$E_{\rm Had}/E_{\rm Em} < 0.125$	0.010
$E^{\rm Iso}_{\rm R=0.4} < 2.0 + 0.02 \cdot (E_T - 20)$	0.647 GeV
$N_{\rm trks} = 0$ or $N_{\rm trks} = 1$ and $p_T < 1.0 + 0.005 \cdot E_T$	$N_{\rm trks} = 0$
$\sum P_T$ of tracks in a 0.4 cone $< 2.0 + 0.005 \cdot E_T$	0.913 GeV/c
$E^{\rm cluster}_{\rm 2nd\ strip\ or\ wire} < 2.34 + 0.01 \cdot E_T$	$E^{\rm cluster}_{\rm 2nd\ strip} = 0.530 GeV$ $E^{\rm cluster}_{\rm 2nd\ wire} = 1.157 GeV$
CES χ^2	3.86
Photon 2	
$E_T > 30$ GeV	46.02 GeV
$\lvert X_{\rm CES}\rvert < 21$ cm	-10.48 cm
9 cm$< \lvert Z_{\rm CES}\rvert < 230$ cm	43.73 cm
Central	$\eta_{\rm det} = 0.235$ $\phi = 3.07$
$E_{\rm Had}/E_{\rm Em} < 0.125$	0.065
$E^{\rm Iso}_{\rm R=0.4} < 2.0 + 0.02 \cdot (E_T - 20)$	0.508 GeV
$N_{\rm trks} = 0$ or $N_{\rm trks} = 1$ and $p_T < 1.0 + 0.005 \cdot E_T$	$N_{\rm trks} = 0$
$\sum P_T$ of tracks in a 0.4 cone $< 2.0 + 0.005 \cdot E_T$	0.424 GeV/c
$E^{\rm cluster}_{\rm 2nd\ strip\ or\ wire} < 2.34 + 0.01 \cdot E_T$	No 2nd Cluster
CES χ^2	1.78
No Jets	
Global Event Properties	
Number of Vertices	2
$\lvert \sum E_T\rvert$	230.5 GeV
$\not\!\!E_T$	54.98 GeV
$\phi(\not\!\!E_T)$	2.60
Optimal Cut Variables	
$\not\!\!E_T\ Significance$>3	19
H_T>200 GeV	207.5 GeV
$\Delta\phi(\gamma_1, \gamma_2)<\pi - 0.15$ rad	2.89 rad

Table 15: The photon, jet, vertex selection and global event cuts, the optimization cuts and their values for event 201674, 3054218.

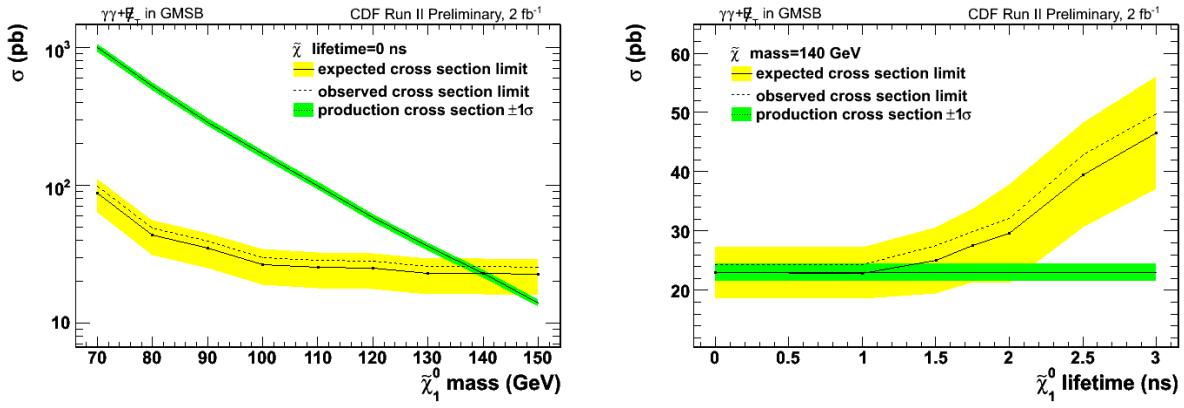

(a) (b)

Figure 12: The predicted and observed cross section limits as a function of the $\tilde{\chi}_1^0$ mass at a lifetime of 0 ns (a) and as a function of the $\tilde{\chi}_1^0$ lifetime at a mass of 140 GeV/c^2 (b). Indicated in green is the 8.0% uncertainty-band for the production cross section (see Table 11), in yellow the RMS variation in the expected on the cross section limit.

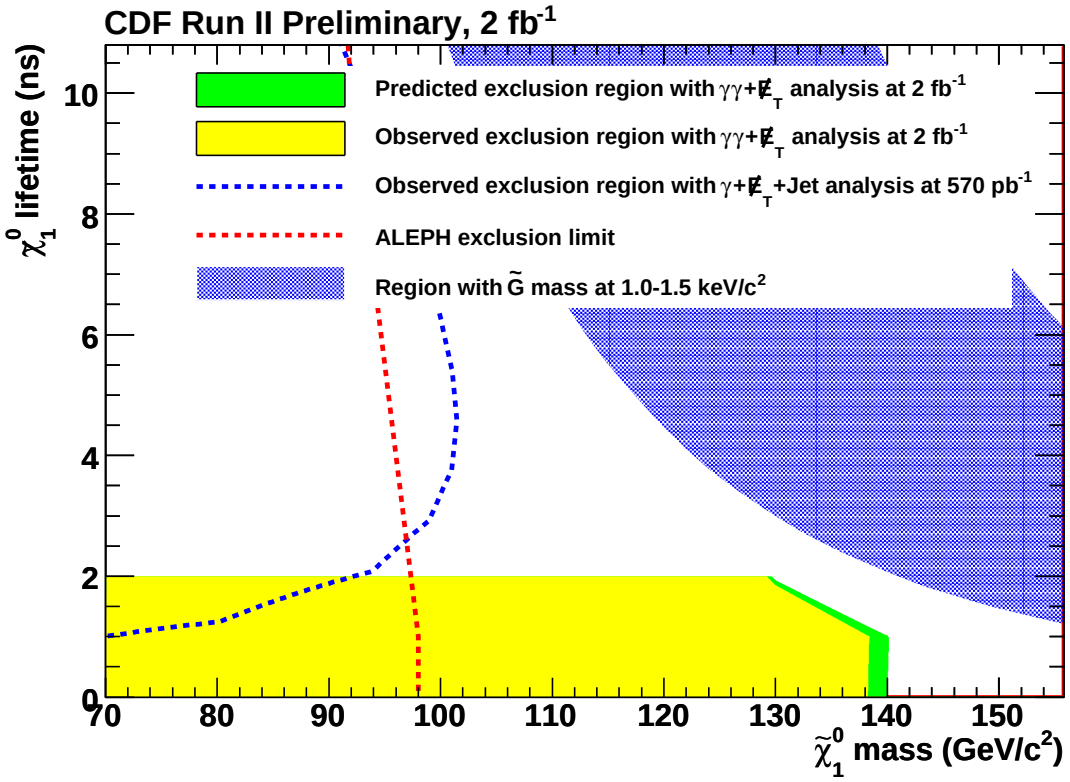

(a)

Figure 13: The predicted and observed exclusion region along with the limit from ALEPH/LEP [9] and delayed photon analysis [16]. We have a mass reach of 140 GeV/c^2 (predicted) and 138 GeV/c^2 (observed) at the lifetime up to 1 ns. The blue shaded band shows the parameter space where $1 \leq m_{\tilde{G}} \leq 1.5\ keV/c^2$, favored in cosmologically consistent models.

8 Conclusions and Prospects for the future

We have set limits on GMSB models using the $\gamma\gamma + \not\!\!E_T$ final state. Candidate events were selected based on the new $\not\!\!E_T$ resolution model technique, the EMTiming system and a full optimization procedure. We found 1 event using 2.03 fb^{-1} of data in run II which is consistent with the background estimate of 0.62±0.29 events from the Standard Model expectations. We showed exclusion regions and set limits on GMSB models with a $\tilde{\chi}_1^0$ mass reach of 138 GeV/c^2 at a $\tilde{\chi}_1^0$ lifetime of 0 ns. Our results extend the world sensitivity to these models.

To investigate the prospects of a search at higher luminosity we calculate the cross section limits assuming all backgrounds scale linearly with luminosity while their uncertainty fractions remain constant. Figure 14 shows the predicted exclusion region for a luminosity of 3 and 10 fb^{-1}.

For higher lifetimes (above ∼2 ns) the next generation delayed photon analysis will extend the sensitiviy and then will combine these results for completeness.

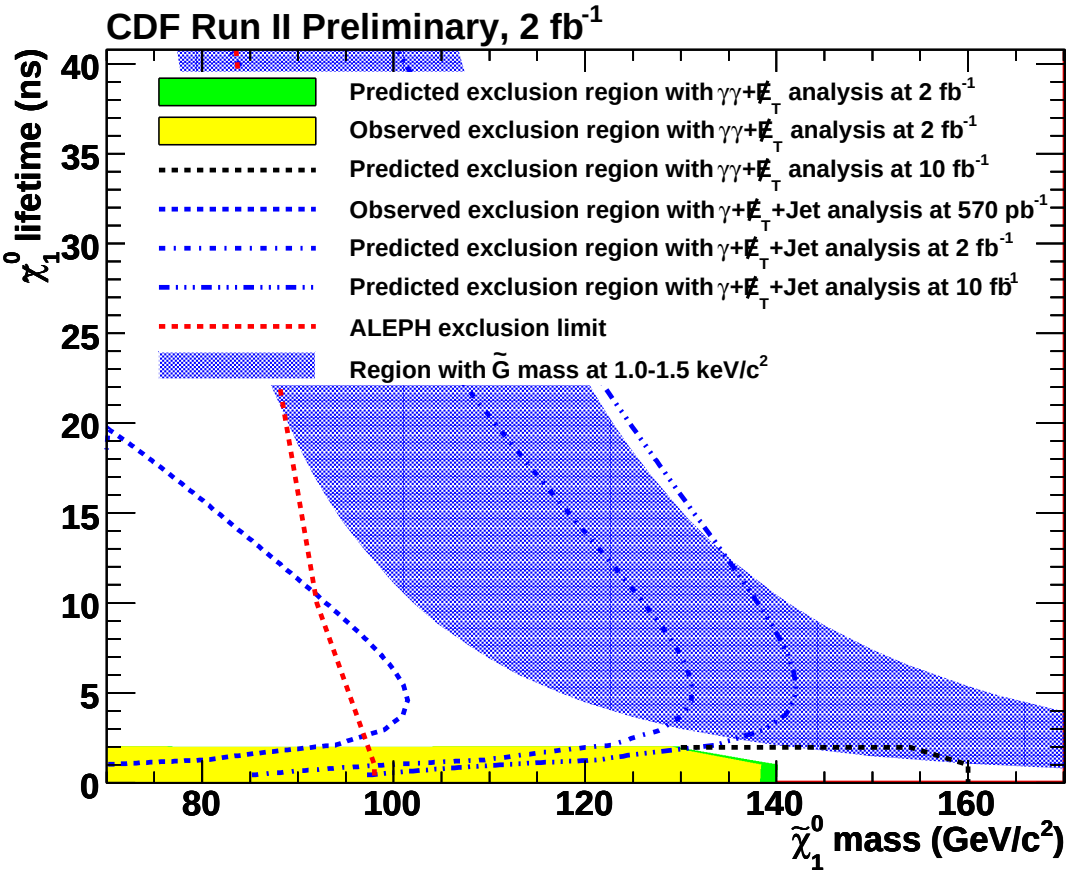

(a)

Figure 14: The black dashed line shows the prediction of the exclusion region limit after a scaling of the background prediction and the uncertainties for a luminosity of 10 fb^{-1}. The blue dashed lines show the prediction of the exclusion region limits from the delayed photon analysis for a luminosity of 2 fb^{-1} and 10 fb^{-1} respectively.

References

[1] See for example S. Ambrosanio, G. L. Kane, G. D. Kribs, S. P. Martin and S. Mrenna, Phys. Rev. D **54**, 5395 (1996) or C. H. Chen and J. F. Gunion, Phys. Rev. D **58**, 075005 (1998).

[2] H. Baer *et al.*, FERMILAB-Pub-00/251-T, S. Dimopoulos *at al.*, SLAC-PUB-7236 (1996).

[3] J. L. Feng and T. Moroi, Phys. Rev. D **70**, 075019 (2004).

[4] P. Bode, J. Ostriker and N. Turok, Astrophys. J. **556**, 93 (2001).

[5] CDF Collaboration, F. Abe *et al.*, Phys. Rev. Lett. **81**, 1791 (1998); Phys. Rev. D **59**, 092002 (1999).

[6] P. Wagner and D. Toback, Phys. Rev. D **70**, 114032 (2004).

[7] CDF Collaboration, D. Acosta *et. al.*, Phys. Rev. D **71**, 031104 (2005).

[8] B. C. Allanach *et. al.*, Eur. Phys. J. C**25**, 113 (2002).

[9] ALEPH Collaboration, A. Heister *et. al.*, Eur. Phys. J. C **25**, 339 (2002); A. Garcia-Bellido, Ph.D. thesis, Royal Holloway University of London (2002) (unpublished), arXiv:hep-ex/0212024.

[10] S. Ambrosanio, G. L. Kane, G. D. Kribs, S. P. Martin and S. Mrenna, Phys. Rev. D **54**, 5395 (1996).

[11] The remaining processes produce slepton pairs that also decay to pairs of $\tilde{\chi}_1^0$: τ_1 ($\sim 9\%$), e_R ($\sim 7\%$), μ_R ($\sim 7\%$).

[12] PYTHIA: T. Sjöstrand, L. Lönnblad and S. Mrenna, arXiv:hep-ph/0108264 (2001); *cdfsoft* 6.1.2 has PYTHIA version 6.216. *cdfSim*: G.S. Sganos, Tutorial on cdfSim. We modified it for the simulation of the EMTiming system [29]. It further includes a bug-fix of the tracking code to simulate the CES response to photons from displaced vertices correctly and a patch by A. Scott to include decay products of displaced $\tilde{\chi}_1^0$ in the detector simulation [30].

[13] W. Beenakker, *et al.*, Phys. Rev. Lett. **83**, 3780 (1999).

[14] P. Simeon and D. Toback, "An Advantage of Setting Cross Section Limits on the Total Production Mechanism When Multiple Processes Produce the Same Final State," CDF Note 7084 (2006).

[15] DØ Collaboration, Phys. Rev. Lett. **80**, 442 (1998).

[16] CDF Collaboration, A. Abdulencia *et. al.*, Phys. Rev. Lett **99**, 121801 (2007); CDF Collaboration, T.Aaltonen *et. al.*, Phys. Rev. D **78**, 032015 (2008). S. P. Martin and S. Mrenna, Phys. Rev. D **54**, 5395 (1996).

[17] M. Goncharov *et. al.*, "The Timing System for the CDF Electromagnetic Calorimeters," CDF Note 7918 (2005), NIM A**565**, 543 (2006).

[18] DØ Collaboration, V.M. Abazov *et. al.*, Phys. Lett. B **659**, 856 (2008).

[19] R. Culbertson, M. Goncharov, and A. Pronko, "Search for Anomalous Production of $\gamma\gamma + \not\!\!E_T$ Events in 2 fb^{-1} of Data", CDF note 9184.

[20] S. Jindariani *et al.,* "Luminosity Uncertainty for Run 2 up until August 2004", CDF note 7446.

[21] http://www-cdf.fnal.gov/internal/physics/photon/goodrun.html, file goodrun_v17_pho_02.txt.

[22] http://www-cdf.fnal.gov/internal/dqm/goodrun/good.html, the script SAMLumi.ksh to compute luminosities for a given goorun list and dataset.

[23] Ray Culbertson *et al.,* "Search for Anomalous $\gamma\gamma + \not\!\!E_T$ Production and Limits on GMSB Models", CDF note 6389.

[24] http://www-cdf.fnal.gov/tiki/tiki-index.php?page_ref_id=57, Stntuple dev_243 build instructions.

[25] M. Goncharov *et al.,* "Methods for Determining the Photon Event Rates and Timing Distributions for Searches with Final State Photons", CDF note 7960.

[26] R. Culbertson, A. Pronko, and Shin-Shan Eiko Yu, "The Probability of an Electron Faking an Isolated Prompt Photon in CEM", CDF note 8220.

[27] M. Goncharov *et al.,* "Discrimination of Beam Halo and Cosmic Rays as a Source of Photon Candidates", CDF note 8409.

[28] http://www-cdf.fnal.gov/physics/ewk/mc_samples.html 6 6 6 6 6, 8 7 7 7, 10, 37 8, 9, 37, 38, 39 9, 42, 85 9 10 10 20 19 20 24.

[29] M. Goncharov, V. Krutelyov, D. Toback and P. Wagner, "Resolution and Simulation of the EMTiming System," CDF Note 7928 (2006).

[30] M. Goncharov, D. Toback and P. Wagner, "Identification Efficiencies for Photons from Heavy, Long-Lived, Neutral Particles," CDF Note 7929 (2006).

[31] The ISASUGRA output is converted to PYTHIA using a script by A. Scott.

[32] R. Rossin, CDF Detector Lectures: "Systematics on the Luminosity Measurement," http://fcdfwww.fnal.gov/internal/WebTalks/Archive/0410/041007_clclum_detector_lecture/04_041007_clclum_detector_lecture_Roberto_Rossin_1_RobertoCLC_detector-04-10-07.pdf; S. Klimenko, J. Konigsberg and T. M. Liss, FERMILAB-FN-0741 (2003).

[33] C. Group, R. Culbertson, and J. Ray, "Photon Efficiency Scale Factor, " CDF Note 9429 (2008).

[34] M. McFarlane, H. Bachacou, J. Nielsen, and W. Yao, "Study of High p_T Lepton Identification Efficiency Scale Factor and Related Cuts and Parameters in 5.3.3, " CDF Note 7682 (2005).

[35] http://www-cdf.fnal.gov/internal/physics/joint_physics/agenda/20050527-minutes.html

[36] http://www-cdf.fnal.gov/internal/physics/top/jets/systematics.html

[37] O. Gonzalez and C. Rott, "Uncertainties due to the PDFs for the gluino-sbottom search," CDF Note 7051 (2005).

[38] M. Griffiths *et. al.*, "Searches for Chargino and Neutralino in the e+e/mu+e/mu with 1 fb-1 of data," CDF Note 8389 (2006).

[39] see e.g. W. Beenakker, *et al.*, Nucl. phys. B **492**, 51 (1997); Prospino 2.0: http://www.ph.ed.ac.uk/∼tplehn/ prospino/prospino.html

[40] E. Boos, A. Vologdin, D. Toback and J. Gaspard, Phys. Rev. D **66**, 013011 (2002). J. Conway, CERN Yellow Book Report No. CERN 2000-005 (2000), p. 247.